D4_7 Scientific Basis of FIDUCEO FCDRs

C.Merchant[1], G.Holl[1], J.Mittaz[1], R.Phipps[1], M. Taylor[1], R. Quast[2], Y.Govaerts[3], V. John[4], F.Ruethrich[4], R.Roebeling[4], M.Burgdorf[5], I.Hans[5], E. Woolliams[6], T.Block[7]

[1] University of Reading
[2]FastOpt
[3]Rayference
[4]Eumetsat
[5]University of Hamburg
[6]National Physical Laboratory
[7]Brockmann Consult

29/8/2019

FIDUCEO has received funding from the European Union's Horizon 2020 Programme for Research and Innovation, under Grant Agreement no. 638822

1 Contents

2 Introduction 3
2.1 Scope 3
2.2 Version Control 3
2.3 Glossary 3
2.4 Executive Summary 3
3 Background 5
3.1 FIDUCEO Scientific Standpoint 5
3.2 Uncertainty estimation for climate data records 5
3.3 Finding satellite match-ups 9
3.4 Harmonisation 9
4 Meteosat Visible Infrared Imager (MVIRI) FCDR 14
4.1 Climate Data Records from Meteosat First Generation Part I: Simulation of Accurate Top-of-Atmosphere Spectral Radiance over Pseudo-Invariant Calibration Sites for the Retrieval of the In-Flight Visible Spectral Response 15
4.2 Climate Data Records from Meteosat First Generation Part II: Retrieval of the In-Flight Visible Spectral Response 17
4.3 Climate Data Records from Meteosat First Generation Part III: Recalibration and Uncertainty Tracing of the Visible Channel on Meteosat-2–7 Using Reconstructed, Spectrally Changing Response Functions 20
5 Microwave Radiometer FCDR 22
5.1 The Moon as a photometric calibration standard for microwave sensors 23
5.2 Inter-channel uniformity of a microwave sounder in space 25
5.3 Noise performance of microwave humidity sounders over their lifetime 28
5.4 An Uncertainty Quantified Fundamental Climate Data Record for Microwave Humidity Sounders 29
5.5 Disk-Integrated Lunar Brightness Temperatures between 89 and 190 GHz 30
5.6 Onboard Radio Frequency Interference as the Origin of Inter-Satellite Biases for Microwave Humidity Sounders 32
6 High-resolution Infrared Sounder (HIRS) FCDR 33
6.1 Error covariances in High-resolution Infrared Radiation Sounder (HIRS) radiances 33
6.2 Summary of HIRS Uncertainty & Cross-channel Correlation 34
6.3 Self-emission model 37
6.4 HIRS Harmonisation 37
7 AVHRR FCDR 41

8 References 43

2 Introduction

This report contains highlights of the scientific developments made during FIDUCEO that form the basis of the new Fundamental Climate Data Records (FCDRs) produced by the project.

2.1 Scope

The four FCDRs produced by the project are addressed.

2.2 Version Control

Version	Reason	Reviewer	Date of Issue
1.3	First version	Authors	29 August 2019

2.3 Glossary

AAPP	ATOVS and AVHRR Pre-processing Package
AMSU-B	Advanced Microwave Sounding Unit -B
ATOVS	Advanced TIROS-N Operational Vertical Sounder
AVHRR	Advanced Very High Resolution Radiometer
CDR	climate data record
DMSP	Defense Meteorological Satellite Program
DSV	deep space view
ECV	essential climate variable
EUMETSAT	European Organisation for the Exploitation of Meteorological Satellites
FCDR	fundamental climate data record
IWCT	internal warm calibration target
LECT	local equator crossing time
MHS	Microwave Humidity Sounder
MW	microwave
MVIRI	Meteosat Visible and Infrared Imager
MW	Microwave
NEdT	Noise equivalent differential temperature
NetCDF	Network Common Data Format
NOAA / CLASS	National Oceanographic and Atmospheric Administration / Comprehensive Large-Array Stewardship System
NWP	numerical weather prediction
PICS	Pseudo-invariant calibration site
RFI	radio frequency interference
SNO	simultaneous nadir overpass
SSMT-2	Special Sensor MicrowaveWater Vapor Profiler
UTH	upper tropospheric humidity
HIRS	High-resolution Infrared Sounder

2.4 Executive Summary

Approaches from metrology can assist earth observation (EO) practitioners to develop quantitative characterisation of uncertainty in EO data. This is necessary for the credibility of

statements based on Earth observations in relation to topics of public concern, particularly climate and environmental change.

This report gives highlights of the application of metrological uncertainty analysis to historical Earth observations from satellites in FIDUCEO, in the context of four FCDRs: for MVIRI, microwave sounders, HIRS and AVHRR. Fuller details are given in peer-reviewed papers, to which this report refers.

Significant scientific developments in FIDUCEO illustrated here include:

- The specification of a user-orientated tri-partite categorisation of uncertainty (§3.2)
- The implementation of this tri-partite uncertainty categorisation in FCDRs (§3.2)
- Practical techniques for multi-sensor match-ups (§3.3)
- The clarification of the concept of harmonisation of FCDR records as re-calibration respecting true instrument differences (§3.4)
- Methods for multi-mission harmonisation (microwave, HIRS, AVHRR) using matches and cutting edge large-data minimisation techniques (accounting for correlation) (§3.4)
- New methods for spectral response function estimation as part of harmonisation (MVIRI) (§4)
- A number of other instrument-specific methods (for microwave, HIRS and AVHRR) for FCDR uncertainty characterisation and harmonisation, showing the fruitfulness of instrument specialists interacting with metrological expertise (all other sections)

The over-arching framework for all FCDR (and CDR) implementation has been published in the peer-reviewed literature (Mittaz et al., 2019), and forms the common basis for the highlights given in this report.

3 Background

3.1 FIDUCEO Scientific Standpoint

An aim of FIDUCEO is to create new Fundamental Climate Data Records for four sensors with clearer information about the uncertainties contained within them, and how these propagate to derived geophysical datasets.

These are problems to which the discipline of metrology, the science of measurement, may contribute solutions. The classic task of metrology is the linking of practical measurements made in science and industry to internationally-defined standards, particularly the Système International d'Unités (SI; e.g. http://www.bipm.org/en/publications/sibrochure/). This endeavour is crucial if empirical measurements made in one time and place are to be interpretable with confidence at a different time or elsewhere. A measurement that has been thus linked to standards is referred to as 'traceable', and the key aspect of traceability is that it allows the intrinsic uncertainty of the measurement relative to standards to be stated. Metrology is therefore deeply engaged with the science and mathematics of uncertainty, and with the understanding and calibration of instruments.

3.2 Uncertainty estimation for climate data records

There are multiple uncertainties that are related to EO, particularly from satellites. These include differences which are attempted to be considered through controlled laboratory experiments before launch. In laboratory metrology, a recognised method for estimating uncertainty is statistical evaluation of repeated measurements. In the case of EO, repeat measurements are generally not available, because of continual variations in sensor state, viewing geometries that repeat only approximately between different satellite overpasses, and because of natural geophysical variability.

A Guide to the Expression of Uncertainty in Measurement (hereafter referred to as GUM), written in 2008 provides guidance on how to express, determine, combine and propagate uncertainty, and is maintained by the Joint Committee for Guides in Metrology (JCGM). This gives definitions of uncertainty as a "parameter, associated with the result of a measurement, that characterizes the dispersion of the values that could reasonably be attributed to the measurand", and error of measurement as the "result of a measurement minus a true value of the measurand". Since the true value of the measurand is unknown, the error associated with the measurement must also be unknown. By analysing the sources of errors associated with an EO measurement, the uncertainty can be evaluated.

Several errors are associated with EO measurements, which must be taken into account. These can be put into two categories according to their nature of origin: Systematic errors and Random errors.

Random errors are errors manifesting independence: the error in one instance is in no way predictable from knowledge of the error in another instance. A complication arises in EO imagery when one instance of a parameter in the radiance measurement function is used in the calculation of the Earth radiance across many pixels. That component of the error in the radiance image is then correlated across pixels, even though the originating effect is random.

Systematic errors are those that could in principle be corrected for if we had sufficient information to do so: that is, they arise from unknowns that could in principle be estimated rather than from chance processes. All systematic errors in EO are structured in that there is a pattern of influence

on multiple data. They include, but are not limited to, effects that are constant for a significant proportion of a satellite mission—i.e. biases, for which the structure is a simple error in common. Categorisation of errors in relation to the characteristics of origin is a long-standing approach, but in FIDUCEO we have developed a categorisation as a scientific basis for FCDRs that is achieves the following in the context of Earth Observation:

- It is user-oriented – i.e., is formulated in the way that EO users need (aligning with the impact on their applications rather than the nature of the origin of errors)
- It is as simple as possible while retaining key information

The FIDUCEO categorisation puts effects into 3 categories which determine their cross-pixel error correlation: Independent errors, structured errors and common errors. The cross-pixel error structure is the key thing a user needs to know when assessing how errors propagate through their application of the FCDR.

Independent errors arise from random effects causing errors that manifest independence between pixels, such that the error in a pixel is in no way predictable from knowledge of the error from a previous pixel retrieval, were that knowledge available. Independent errors therefore arise from random effects operating on a pixel level, the classic example being detector noise.

Structured errors arise from effects that influence more than one measured value in the satellite image, but are not in common across the whole image. The originating effect may be random or systematic (and acting on a subset of pixels), but in either case the resulting errors are not independent, and may even be perfectly correlated across the affected pixels. Since the sensitivity of different pixels/ channels to the originating effect may differ, even if there is perfect error correlation, the error (and associated uncertainty) in the measured radiance can differ in magnitude. Structured errors are therefore complex, and, at the same time, important to understand, because their error correlation properties affect how uncertainty propagates to higher-level data.

Common errors are constant (or approximately so) across the satellite image, and may be shared across the measured radiances for a significant proportion of a satellite mission. Common errors might typically be referred to as biases in the measured radiances. Effects such as the progressive degradation of a sensor operating in space mean that such biases may slowly change.

The reality is that effects arise with a continuum of correlation properties. The tripartite division of uncertainty is the minimum needed to support uncertainty propagation across climate-related scales with some degree of realism. Nonetheless, it remains an approximation into sensor teams have allocated different error effects on the basis of their judgment and sensor knowledge.

Level 1 radiances are typically calculated using an equation similar to:

$$L_{c,l,e} = a_0 + a_1 * C^E_{c,l,e} + a_2 (C^E_{c,l,e})^2 + 0 \qquad (3.1)$$

where: $L_{c,l,e}$ is the calculated Earth radiance for channel c of the pixel at image co-ordinate (l, e); $C^E_{c,l,e}$ is the Earth count for the pixel recorded by the sensor; a0, a1 and a2 are calibration parameters, with $\mathbf{a}^E = [a_0, a_1, a_2]$. Uncertainty in the calculated radiance arises in part from uncertainties in the values of the quantities on the right hand side. In general, there are also other effects expected to have zero mean that contribute uncertainty in the calculated radiance, which gives the +0 term at the end of the equation. Calibration parameters are determined by in-flight calibration data of pre-specified targets, plus pre-flight sensor specific measurements. Sensors are generally reasonably linear, so a2 is often small.

Uncertainty analysis in the GUM begins with modelling the measurement, i.e. linking the measurand to the input quantities from which it is derived. A generic measurement model for a L1 radiance would be

$Y = f(X_1, X_2, \ldots, A) + \Delta$ (3.2)

where: $X_1, X_2, \ldots$ are input quantities; A is the vector of calibration parameters (which are also input quantities but are usefully distinguished); and Δ is an input quantity introduced to represent any inadequacy of the function f to represent all phenomena that affect the measurand. The equations, such as equation (3.2), used to populate L1 products, evaluate the measurand (radiance) using estimates of the input quantities. In the GUM, the convention is for estimates to be represented with the lower-case characters corresponding to the quantities written in upper case. Equation (3.1) is then seen as a particular case of the expression by which the measurand is estimated:

$y = f(x_1, x_2, \ldots, a) + \delta$ (3.3)

where the input estimates include the recorded sensor counts, etc. This clarifies the meaning of the '+ 0' term previously introduced: 0 is our best estimate of δ, which is the expectation of Δ (assuming we are using the best measurement model we can formulate).

The uncertainty in the measured value is derived from the evaluation of the uncertainty in each input estimate. The uncertainty in all input estimates, including calibration parameters and δ is relevant. Evaluation of the uncertainty in y means propagation through the measurement model of these uncertainties (or, strictly, distributions).

The GUM and its supplements describe both the 'Law of Propagation of Uncertainty' (hereafter, LPU) and Monte Carlo methods of uncertainty propagation.

The LPU propagates standard uncertainties for the input quantities through a locally-linear first-order Taylor series expansion of the measurement function to obtain the standard uncertainty associated with the estimate, y, of the measurand. Higher order approximations can be applied if necessary. Monte Carlo methods approximate the input probability distributions by finite sets of random draws from those distributions and propagate the sets of input values through the measurement function to obtain a set of output values regarded as random draws from the probability distribution of the measurand. The output values are then analysed statistically, for example to obtain expectation values, standard deviations and error covariances. The measurement function in this case need not be linear nor written algebraically. Steps such as inverse retrievals and iterative processes can be addressed in this way. The input probability distributions can be as complex as needed, and can include distributions for digitised quantities, which are very common in EO, where signals are digitised for on-board recording and transmission to ground. Monte Carlo methods can provide information about the shape of the output probability distribution for the measurand, deal better with highly non-linear measurement functions and with more complex probability distributions, and can be the only option for models that cannot be written algebraically. The input probability distributions can be as complex as needed, and can include distributions for digitised quantities, which are very common in EO, where signals are digitised for on-board recording and transmission to ground. Uncertainty analyses will use a combination of Monte Carlo methods and the LPU, such as using Monte Carlo methods to determine the uncertainty for a particular quantity, which is then used as an input to LPU in a subsequent uncertainty analysis.

Most radiance measurement function terms are sensitive to one or more effects, and the uncertainty due to each effect needs to be estimated. Quantities not subject to effects include mathematical and physical constants, and agreed reference quantities. In some cases, contributing effects may be estimated separately and then combined, and in other cases, all the effects operative on a single quantity may only be jointly estimated. Many effects are possible in EO: examples at L1 include detector noise, temperature gradients across reference targets, stray light ingress and temperature sensitivity of electronics. The '+ 0' term in a radiance measurement

function represents effects relating to the assumptions underlying the form of the measurement function, e.g. that the sensor response is linear or quadratic in underlying radiance. An example of how this equation is linked to the uncertainties in an EO satellite dataset is given below in equation 3.4-3.6.

$$L_E = a_0 + \frac{a_1 L_T - a_2 \hat{C}_T^2}{\hat{C}_T} \acute{C}_E + a_2 \acute{C}_E^2 + 0 \quad \text{(Equation 3.4)}$$

$$\hat{C}_T = \frac{1}{n} \sum (C_{S,i}\, C_{T,i}) \quad \text{(Equation 3.5)}$$

$$\acute{C}_E = C_S - C_E \quad \text{(Equation 3.6)}$$

where L_E is the Earth radiance, L_T is the estimated radiance of the ICT, $\hat{C}_T$ is the counts observed when looking at the ICT averaged over a number of scanlines (in practice a space-view count C_s minus a target count) and C_E is the Earth-view count (in practice a space-view count minus the Earth-view count) and a_1, a_2, a_3 are calibration parameters that have physical interpretations. A deconstructed version of Equation 3.4 is shown in Figure 3.1.

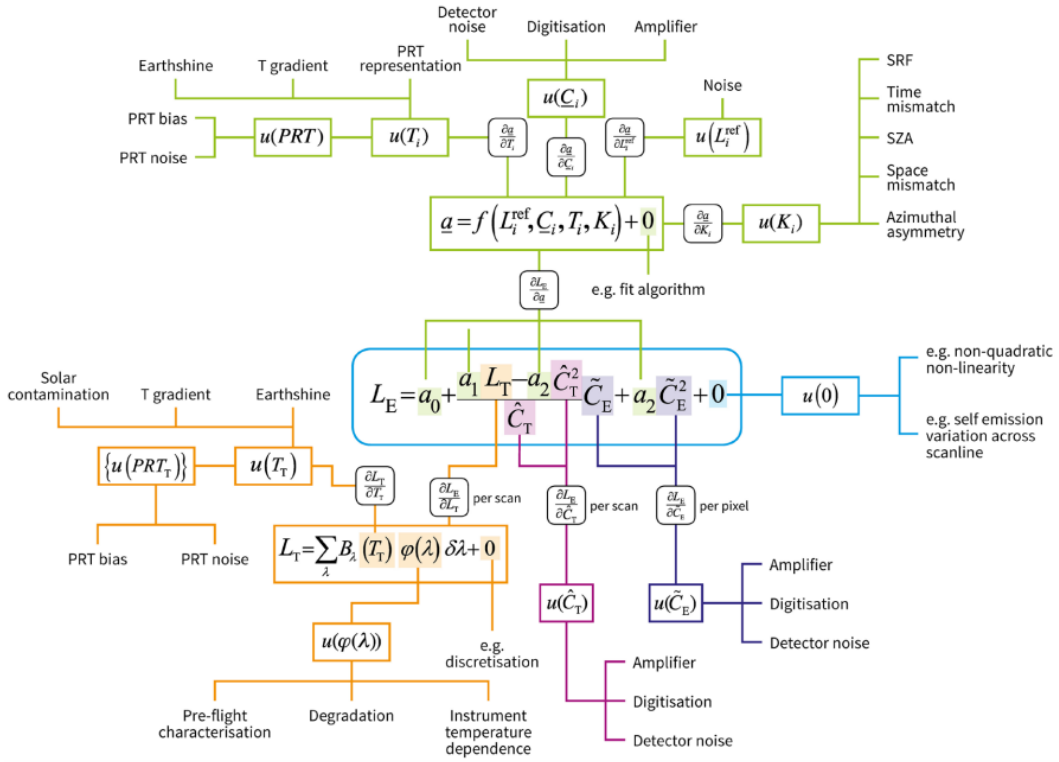

Figure 3.1. Uncertainty analysis diagram for the AVHRR. The AVHRR infrared radiance measurement function is an analytic equation in terms of observed counts and calibration parameters, shown at the centre of the diagram. Each term is addressed by a colour-coded branch that links to an uncertainty model, u(.), for that term that derives from one or more effects, that are noted in the next level of branching. In two cases (namely, the calibration parameter vector a and the calibration-target radiance LT), the term is linked to a secondary measurement function. Links between a term and its uncertainty are labelled with the sensitivity coefficient required to assess the impact of uncertainty in that term to the outcome of the measurement function. Taken from Mittaz et al. 2019.

The uncertainty analysis diagram documents in a visual form the full set of error effects to be analysed and their connections to the measurement function. In the upper half of the diagram are the components related to harmonisation between sensors, whilst the diagram also includes the sensitivity coefficients on each branch that enable the source uncertainties to be propagated to the measurand. Following the metrological approach described above, known sources of systematic errors are removed with best estimations, and the remaining uncertainty is quantified. This approach will lead to both a more accurate climate data record, and improved assessment of a quantitative uncertainty for each retrieval.

3.3 Finding satellite match-ups

A key step in the development of FCDRs is harmonisation, described in the next section. To achieve harmonisation in the case of multi-sensor records from polar-orbiting missions requires matches between sensors. While not a fundamental scientific concept, multi-sensor match-up generation is a technology that is necessary for (some) FCDR production.
The technical/scientific basis for the multi-sensor match-up system is well described in the following paper:
Block, T., Embacher, S., Merchant, C. J. and Donlon, C. (2018) *High performance software framework for the calculation of satellite-to-satellite data matchups (MMS version 1.2).* Geoscientific Model Development, 11 (6). pp. 2419-2427. ISSN 1991-9603

The multisensor matchup system (MMS) allows systematic detection of satellite-based sensor-to-sensor matchups and the extraction of local subsets of satellite data around matchup locations. The software system implements a generic matchup-detection approach and is currently being used for validation and sensor harmonization purposes.
Work in FIDUCEO demonstrated and implemented a general matchup processing system using a novel and fast intersection detection algorithm for polar-orbiting satellite-based sensor overlaps. The time axis approach for acquisition time detection and the use of a novel library for spherical calculations allow performance gains of up to a factor of 3.5 compared to a conservative implementation. A two-step screening system is highly configurable to adapt the matchup process to several scientific requirements. The software is designed to be operated on a parallel cluster environment; tests with up to 200 nodes have been executed successfully. The software has been used for operational processing in a parallel environment, and underpins the data required as input for harmonisation.

3.4 Harmonisation

Harmonisation designates the conceptual framework behind FIDUCEO Fundamental Climate Data Records. A harmonised satellite data series is one where the calibration of all sensors in a series of sensors have been made consistent with a reference dataset which can be traced back to known reference sources, in an ideal case back to SI. Each sensor is calibrated to the reference in a way that maintains the characteristics of that individual sensor such that the calibrated radiances represent the unique nature of each sensor. This means that two sensors which have been harmonised may see different signals when looking at the same location at the same time where the difference is related to known differences in the responses of each sensor such as differences

in the sensor spectral response functions. Harmonisation can be achieved to within an uncertainty that should be estimated, and the harmonisation uncertainty contributes to the component of uncertainty that is common across the whole data record of each sensor.

An explicit methodology to conduct such a harmonised calibration of a series of sensors has not existed before FIDUCEO and was explored and developed by following the errors-in-variables (EIV) idea, which takes into account the uncertainty and error correlation in all sensor telemetry measurements and yields optimised calibration coefficients and an associated calibration error covariance matrix for all sensors (e.g. Newkey 2001).

Figure 1 broadly illustrates the methodology which was developed by the FIDUCEO project to conduct harmonisation within four steps. The first step is to collect dual-sensor matchups where two sensors observe approximately the same Earth target at approximately the same time (Figure 2). These matchup data include all possible reference-to-sensor and sensor-to-sensor pairs. The second step is an assessment of the error covariance of all measurements included with the matchup data and an assessment of the expected matchup radiance differences and their associated uncertainties. The third step consists in a joint optimisation of the calibration models for all sensors. The last step is the evaluation of the calibration error covariance matrix. Figure 3 illustrates an example. The complete methodology is described in detail by Giering *et al.* (2019) and Harris *et al.* (in preparation).

The joint optimisation of sensor calibration models involves the optimisation of sensor calibration coefficients and sensor telemetry corrections. Sensor telemetry data may include several 10 to several 100 million individual measurements and optimising a corresponding number of corrections results in an enormous and highly covariant optimisation problem. The FIDUCEO project demonstrated the feasibility to solve such problems for artificial simulated test cases (Harris *et al.*, in preparation). The demonstrated method, however, did not reach a level that was mature enough to use it to harmonise a series of real Earth Observation sensors. FIDUCEO therefore developed a marginalised EIV variant which reduces the complexity of the optimisation problem without compromising the rigour treatment of measurement uncertainties (Giering *et al.* 2019). Both variants showed similar adequate performance on simulated test data sets.

Applying the marginalised EIV variant to the AVHRR series of sensors yielded a considerable improvement when compared to the nominal radiance calibration. Figure 4 illustrates that jumps and trends in the calibration residuals over time, which are present in the nominal calibration, disappear after harmonisation. The results on the application of the marginalised EIV variant to the AVHRR series of sensors is described in further detail by Giering et al. (2019).

In conclusion, with SI traceable satellites planned and launched in the future, harmonisation will have the potential to establish SI traceability for even heritage instruments, with the ultimate objective to produce SI traceable FCDRs extending over decades, ideally back to the beginning of Earth observation from Space.

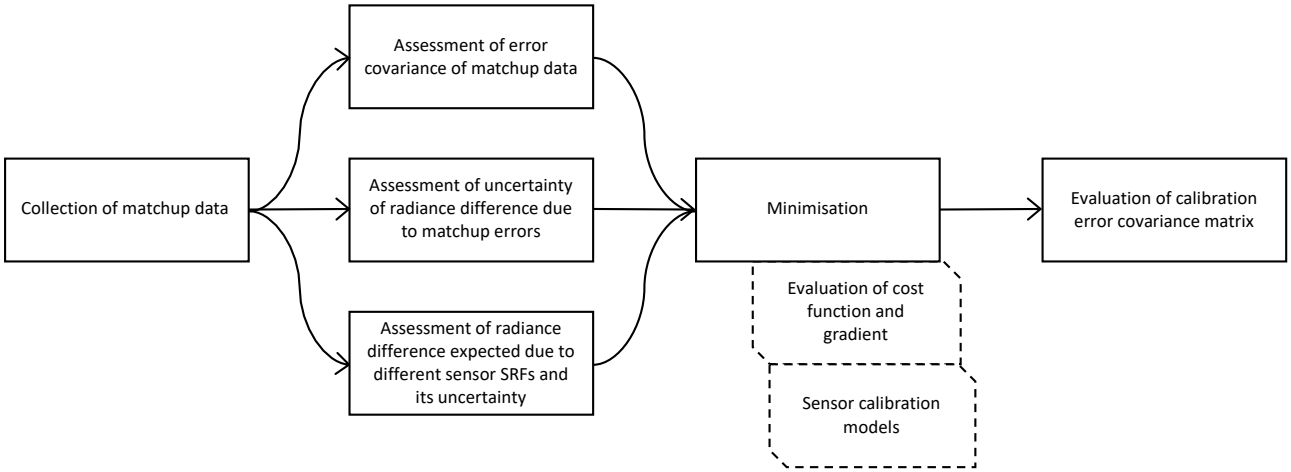

Figure 1: Methodology to conduct harmonisation

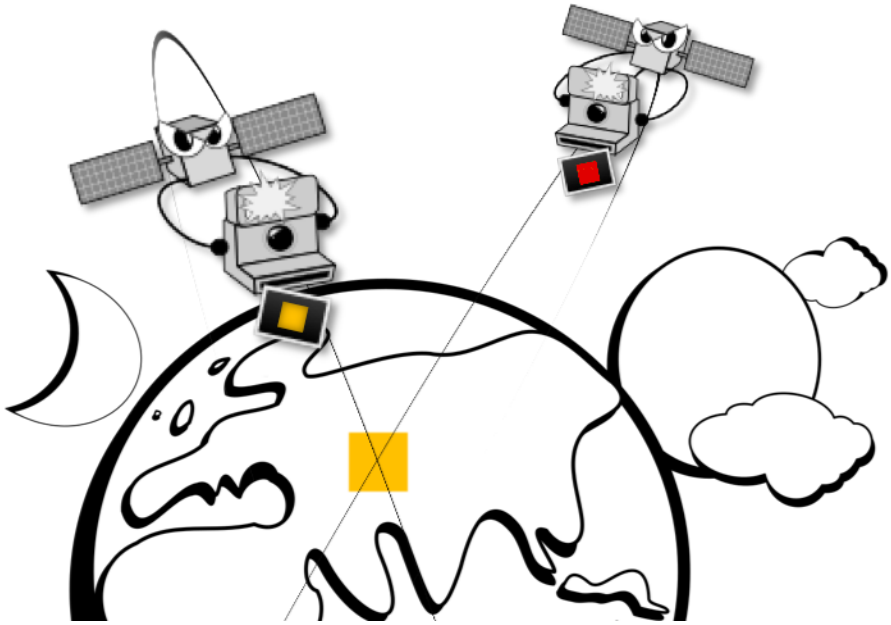

Figure 2: Dual-sensor matchup

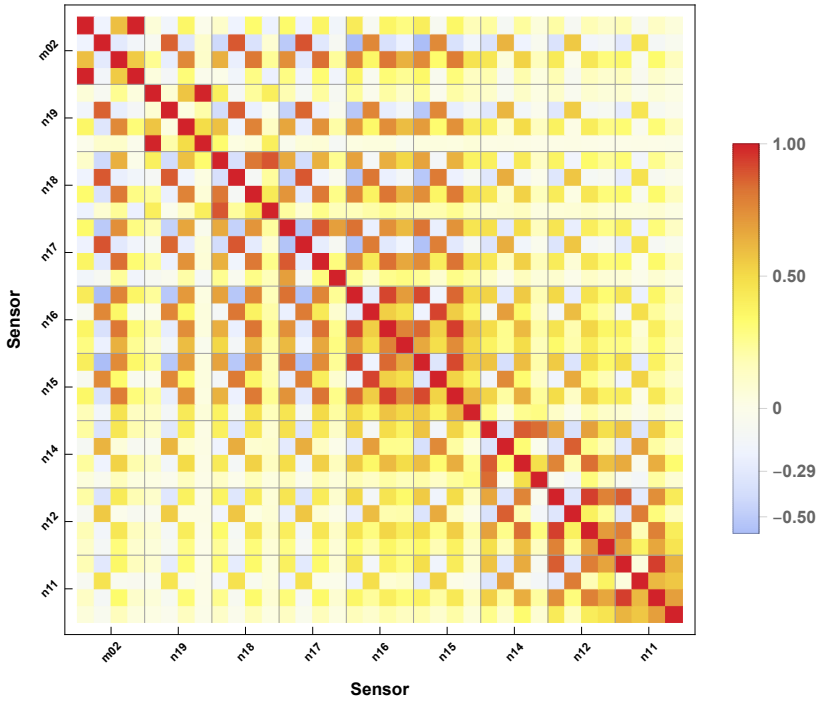

Figure 3: Calibration coefficient error correlation matrix (derived from the calibration error covariance matrix) for the AVHRR series of sensors

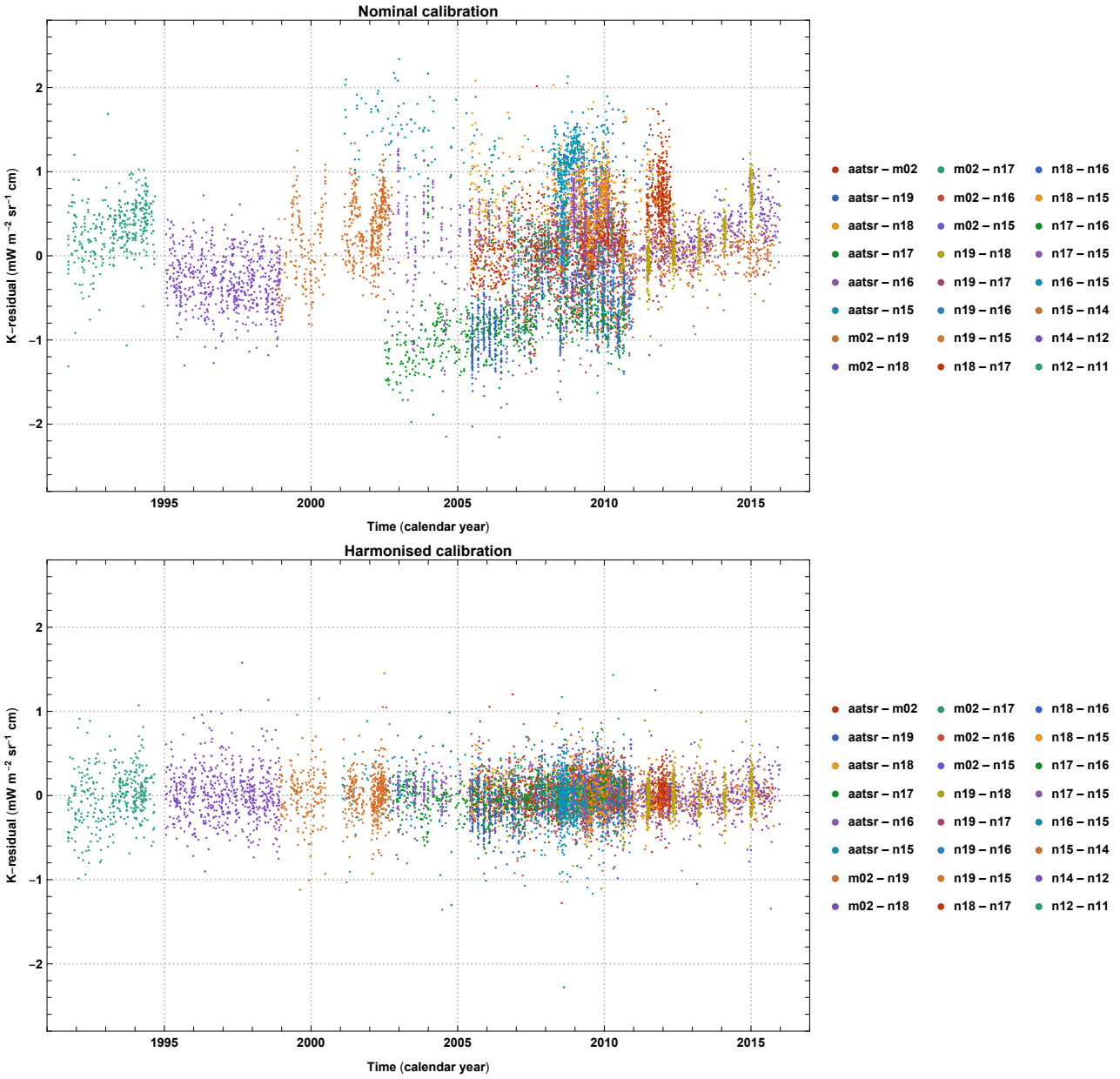

Figure 4: Nominal and harmonised calibration residuals

4 Meteosat Visible Infrared Imager (MVIRI) FCDR

The scientific basis of the MVIRI FCDR is based on the following peer reviewed papers:

1. Paper describing the method to simulate Top Of Atmosphere spectral radiance:
   Govaerts, Yves M., Frank Rüthrich, Viju O. John and Ralf Quast, 2019, Climate Data Records from Meteosat First Generation Part I: Simulation of Accurate Top-of-Atmosphere Spectral Radiance over Pseudo-Invariant Calibration Sites for the Retrieval of the In-Flight Visible Spectral Response, Remote Sens. 2018, 10(12), 1959; https://doi.org/10.3390/rs10121959
2. Paper describing the method to reconstruct spectral response functions:
   Quast, Ralf, Ralf Giering, Yves Govaerts, Frank Rüthrich and Rob Roebeling, 2019, Climate Data Records from Meteosat First Generation Part II: Retrieval of the In-Flight Visible Spectral Response, Remote Sens. 2019, 11(5), 480; https://doi.org/10.3390/rs11050480
3. Paper describing the application of the methods developed to simulate and reconstruct spectral response functions:
   Rüthrich, Frank, Viju O. John, Rob A. Roebeling, Ralf Quast, Yves Govaerts, Emma R. Woolliams and Jörg Schulz, 2019, Climate Data Records from Meteosat First Generation Part III: Recalibration and Uncertainty Tracing of the Visible Channel on Meteosat-2–7 Using Reconstructed, Spectrally Changing Response Functions, Remote Sens. 2019, 11(10), 1165; https://doi.org/10.3390/rs11101165

4.1 Climate Data Records from Meteosat First Generation Part I: Simulation of Accurate Top-of-Atmosphere Spectral Radiance over Pseudo-Invariant Calibration Sites for the Retrieval of the In-Flight Visible Spectral Response[1]

Abstract

Meteosat First-Generation satellites have acquired more than 30 years of observations that could potentially be used for the generation of a Climate Data Record. The availability of harmonized and accurate a Fundamental Climate Data Record is a prerequisite to such generation. Meteosat Visible and Infrared Imager radiometers suffer from inaccurate pre-launch spectral function characterization and spectral ageing constitutes a serious limitation to achieve such prerequisite. A new method was developed for the retrieval of the pre-launch instrument spectral function and its ageing. This recovery method relies on accurately simulated top-of-atmosphere spectral radiances matching observed digital count values. This paper describes how these spectral radiances are simulated over pseudo-invariant targets such as open ocean, deep convective clouds and bright desert surface. The radiative properties of these targets are described with a limited number of parameters of known uncertainty. Typically, a single top-of-atmosphere radiance spectrum can be simulated with an estimated uncertainty of about 5%. The independent evaluation of the simulated radiance accuracy is also addressed in this paper. It includes two aspects: the comparison with narrow-band well-calibrated radiometers and a spectral consistency analysis using SEVIRI/HRVIS band on board Meteosat Second Generation which was accurately characterized pre-launch. On average, the accuracy of these simulated spectral radiances is estimated to be about ±2%.

Conclusions

Past attempts to produce CDRs from MVIRI/VIS band observations have revealed the need to rely on a consistent and accurate FCDR. The lack of accurate pre-launch SRF characterization and its ageing constitute a serious limitation to achieve this objective. The FIDUCEO project main objective is to address these types of limitations. This paper presents an important aspect of the efforts undertaken to generate a consistent FCDR from MVIRI/VIS band observations, namely the generation of reliable TOA radiance spectrum over selected PICSs. The radiative properties of these targets relies on a limited number of parameters that can vary both in space and time, all other parameters such as the atmospheric vertical profiles being kept constant. Uncertainties on these properties are taken into account and propagated into the simulated spectral radiance following the Guide to the Expression of Uncertainty in Measurement.
These TOA spectral radiances were simulated over open ocean, bright desert and DCC for the entire duration of the MFG mission, i.e., from Meteosat-2 data acquired in 1982 to Meteosat-7 data acquired in 2015 to support the MVIRI/VIS band retrieval of these instruments, i.e., the same method is used for the processing of the entire archive. The characterization of all input parameters relies on climate data set with a monthly temporal resolution or are assumed time-invariant. Only meteorological information taken from ECMWF data such as the total column water vapor, ozone or surface wind speed over sea explicitly vary in time. Stratospheric aerosols constitute an exception and fortunately data sets exist to account for these variations. Bright

[1] Based on: Govaerts, Yves M., Frank Rüthrich, Viju O. John and Ralf Quast, 2019, Climate Data Records from Meteosat First Generation Part I: Simulation of Accurate Top-of-Atmosphere Spectral Radiance over Pseudo-Invariant Calibration Sites for the Retrieval of the In-Flight Visible Spectral Response, Remote Sens. 2018, 10(12), 1959; https://doi.org/10.3390/rs10121959

desert surface reflectance, ocean salinity and DCC water droplet/ice crystal radius are assumed invariant because of PICS intrinsic nature. A single radiance spectrum can be simulated with an estimated uncertainty of about 5%.
Significant efforts were dedicated to the independent verification of simulated TOA radiance accuracy. A two-fold approach was followed. First, the accuracy of the simulation over bright desert is estimated against well-calibrated modern instruments. The consistency with simulations over open ocean and DCC is performed in a second step using the SEVIRI/HRVIS band on board MSG-3. This evaluation demonstrated that, on average, the simulated spectral radiance uncertainty can be reduced to about 2% when many observations are considered. This value is comparable to results obtained by other studies [Sterckx et al. (2013), Chen et al. (2015), Chen et al. (2014)]. A similar verification performed on Meteosat-7 data confirmed the issue with the characterization of the MVIRI/VIS band SRF. The outcome of this paper is a key result for the reconstruction of the in-flight SRF and the recalibration of MVIRI data described in companion papers [Quast et al. (2019), Ruethrich et al. (2019)].

4.2 Climate Data Records from Meteosat First Generation Part II: Retrieval of the In-Flight Visible Spectral Response[2]

Executive summary

On the precondition that accurate reference top-of-atmosphere spectral radiance simulations over several types of pseudo-invariant calibration sites (PICS) have been established (Govaerts et *al.* 2018) a post-flight characterisation of the in-flight MVIRI Visible spectral response and its spectral degradation over time appears feasible, in principle. An explicit methodology to achieve such a post-flight characterisation, however, has not existed before FIDUCEO and were to explore and develop.

In retrospective, demonstrated evidence for a questionable prelaunch characterisation of the Visible spectral response function of the MVIRI sensors on-board the Meteosat First Generation (MFG) of geostationary satellites had been available for 20 years (Govaerts 1999) and evidence for spectral degradation of the sensor spectral response functions for 15 years (Govaerts *et al.* 2004). Due to the lack of knowledge on the sensor spectral response functions, the calibration of the MVIRI Visible channel, though sufficient for weather prediction, was not accurate enough for climate applications. And despite several attempts to improve the characterisation and calibration of the MVIRI Visible channel (Decoster *et al.* 2013a, 2013b, 2014) the problem of inadequate sensor calibration was not solved.

The post-flight characterisation of the in-flight MVIRI Visible spectral response had to solve two essential problems. Firstly, to estimate the spectral response before launch of the sensor and, secondly, to estimate the degradation thereof in flight. FIDUCEO tackled both problems by means of a newly developed metrologically sound method for retrieving the Visible spectral response from matchups of PICS image pixels with reference data sets of simulated top-of-atmosphere spectral radiance (Quast *et al.* 2019). Calibration sites included bright desert, open ocean and deep convective cloud targets. The absolute instrument spectral response function was decomposed into generalised Bernstein basis polynomials and a degradation function, which is based on plain physical considerations and able to represent typically observed spectral ageing patterns. Based on based on state-of-the-art inverse problem theory (Tarantola 2005) the method specifies retrieval uncertainties in terms of an error covariance matrix, which is projected from model parameter space into the spectral response function domain and range. The spectral response characterisation considers target type-specific biases due to biases in, e.g., the selection of PICS target pixels or the spectral radiance simulation explicitly. The method was tested with artificial and well-comprehended observational data from the similar Spinning Enhanced Visible and Infrared Imager on-board the Meteosat Second Generation of geostationary satellites and has retrieved meaningful results for all MFG satellites apart from Meteosat-1, which was not available for analysis. Obtained model-to-observation residuals indicate that a stability in tune with the Global Climate Observing System's requirements on the reflected TOA Earth Radiation Budget product is achievable. The actual calibration of the Visible channel of the MVIRI instruments on-

[2] Based on: Quast, Ralf, Ralf Giering, Yves Govaerts, Frank Rüthrich and Rob Roebeling, 2019, Climate Data Records from Meteosat First Generation Part II: Retrieval of the In-Flight Visible Spectral Response, Remote Sens. 2019, 11(5), 480; https://doi.org/10.3390/rs11050480

board MFG satellites using the here-retrieved, spectrally changing response functions, provides a further assessment of applicability and stability (Rüthrich *et al.* 2019).

Figure 5 illustrates the Visible spectral response functions retrieved for Meteosat 2-7. Blue curves mark the smoothed prelaunch spectral response function scaled to prelaunch calibration. Yellow, purple and green curves mark the retrieved absolute spectral response function near the beginning, in the middle and near the end of the instrument lifetime. Coloured shading indicates the uncertainty associated with a curve. Grey dots and stripes illustrate the prior probability distribution over the model space assumed for the retrieval. Red dots mark scaled prelaunch measurements. Figure 6 shows an example of the absolute spectral error correlation matrix (derived from the spectral error covariance matrix) associated with the retrievals.

FIDUCEO provides the community with the retrieved in-flight MVIRI Visible spectral response characterisation through a public repository on GitHub (Figure 7). For each MFG satellite, the retrieved Visible spectral response function and its spectral error covariance matrix are provided for certain days of the year (every 45 days). Applicable spectral response and error covariance are also included with each item of the MVIRI Fundamental Climate Data Record.

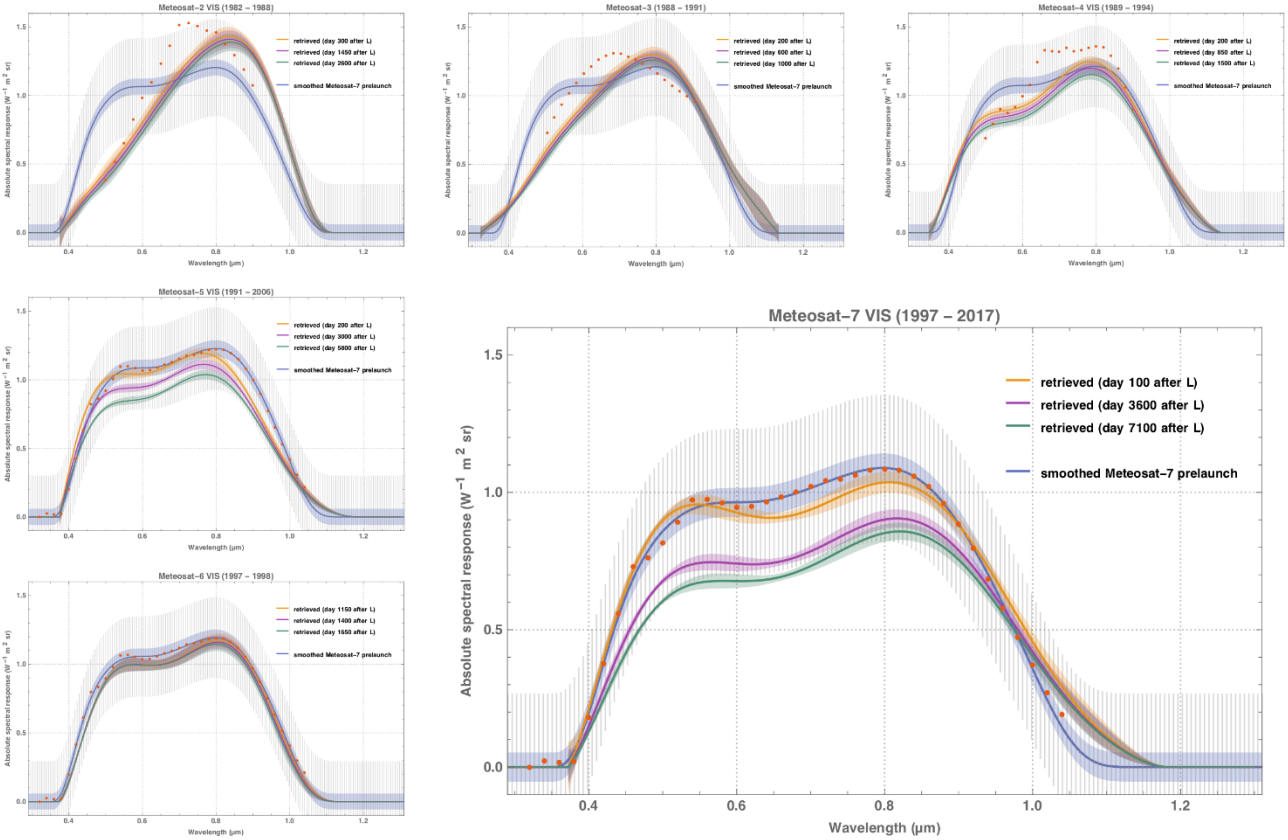

Figure 5: Absolute spectral response functions retrieved for the Visible channel of the radiometers on-board MFG satellites

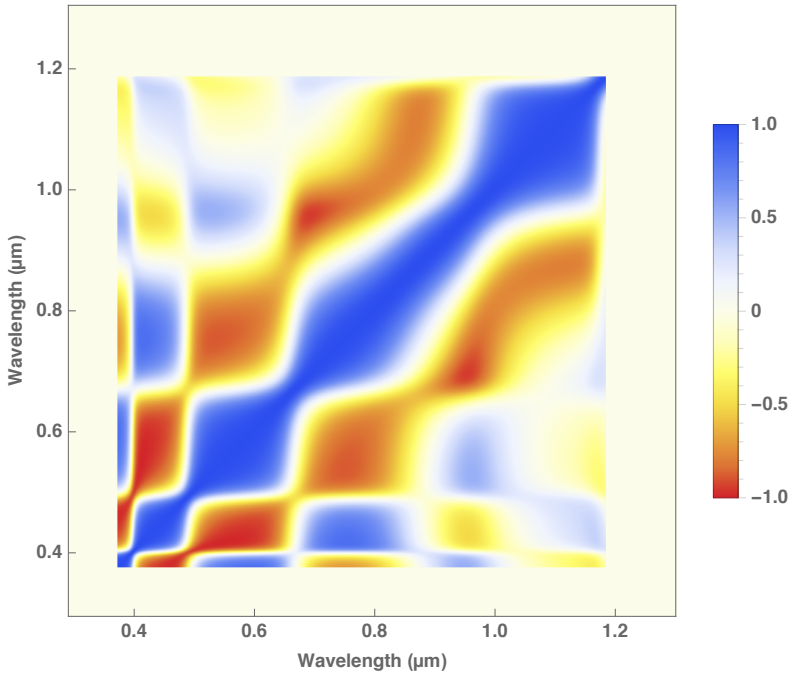

Figure 6: Spectral error correlation matrix of the retrieved Meteosat-7 MVIRI Visible spectral response

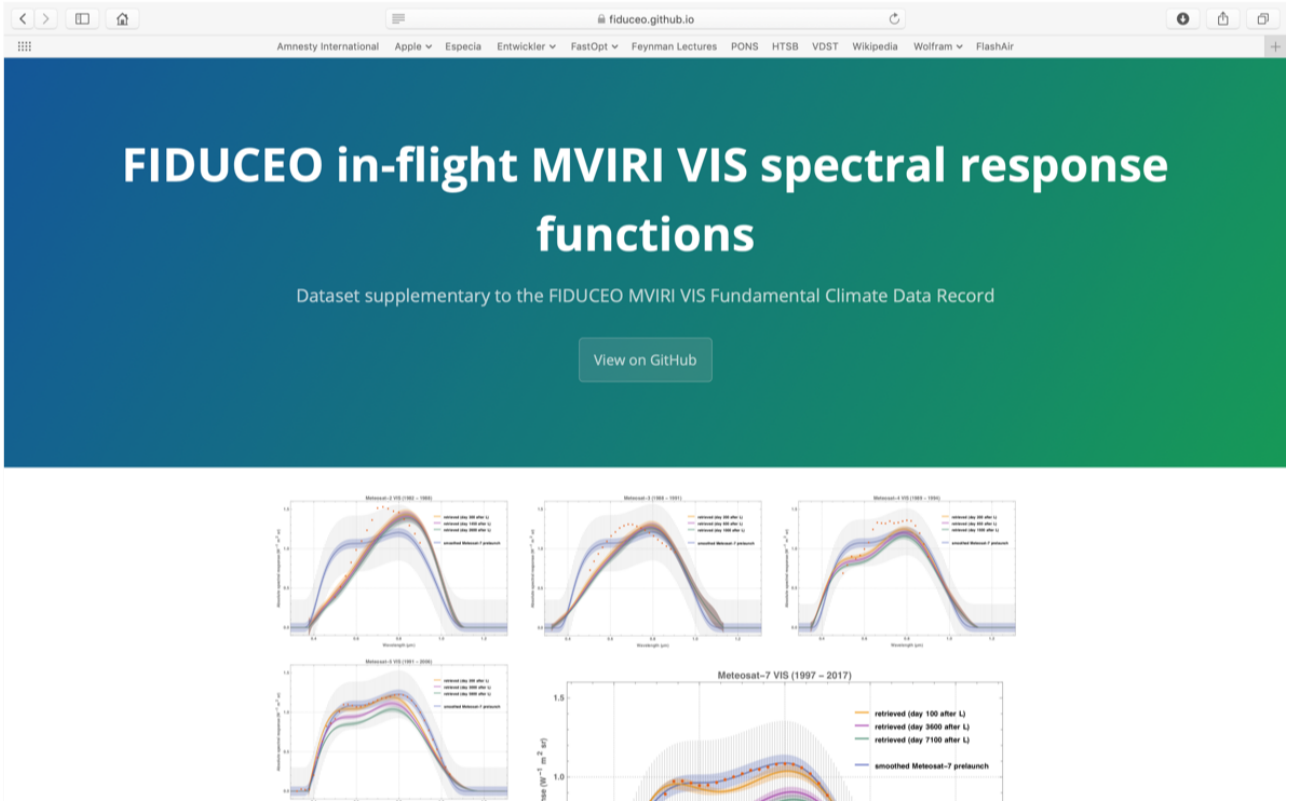

Figure 7: Public repository of MVIRI Visible spectral response function on GitHub

4.3 Climate Data Records from Meteosat First Generation Part III: Recalibration and Uncertainty Tracing of the Visible Channel on Meteosat-2–7 Using Reconstructed, Spectrally Changing Response Functions[3]

Executive Summary

The reconstructed spectral response functions (sections above) provide the necessary precondition for a thorough recalibration of the MVIRI data record. MVIRI has flown onboard Meteosat First Generation (MFG) satellites between 1982 and 2017. It has served the weather forecasting community with measurements of "visible", "infra-red" and "water vapour" radiance in near real-time. The precision of the pre-launch sensor spectral response function (SRF) characterisation, particularly of the visible band of this sensor type, improved considerably with time, resulting in higher quality radiances towards the end of the MFG program. Despite these improvements, the correction of the degradation of this sensor has remained a challenging task and previous studies have found the SRF degradation to be faster in the blue than in the near-infrared part of the spectrum. With these limitations, the dataset was not fit for climate studies in the past.

In order to provide a data record that is suited for climate studies, the Horizon 2020 project "FIDelity and Uncertainty in Climate-data records from Earth Observation" addresses four aspects for the realisation of a long-term, stable and ready-to-use MVIRI visible channel FCDR: (i) the improvement of the instrument characterisation though the use of reconstructed SRFs, (ii) the application of a consistent recalibration methodology, (iii) the quantification of traceable uncertainties using metrological techniques, and (iv) the validation of the performance of the FCDR using reference datasets. The metrological analysis, the recalibration results and the resulting consolidated FCDR were presented in Rüthrich et al. (2019).

While the satellite only collects dimensionless digital counts, the FCDR provides the top of atmosphere bidirectional reflectance factor of the MVIRI VIS band ($\tilde{R}$) that is centered around 0.7µm. It is computed from the digital counts ($\bar{C}_E$) using the measurement equation (Equation 1):

Equation 1

$$\tilde{R} = \frac{\pi d^2}{\tilde{E}_{0,sun}\cos(\theta)}[(\bar{C}_E - \bar{C}_S)(a_0 + a_1 Y + a_2 Y^2)]$$

Where $\bar{C}_S$ is the dark signal level in digital counts, averaged over deep space pixel, θ is the solar zenith angle, $\tilde{E}_{0,sun}$ is the band-integrated solar irradiance and a_X are the calibration parameters that describe the calibration coefficient in a second order polynomial along with the fractional years since launch Y. The reconstructed SRFs improve the trueness of the band integrated solar irradiance and, during the recalibration, the trueness of the calibration parameters. Remaining uncertainties in all parameters of the measurement equation are determined at each instance and propagated, at pixel level, from the underlying physical effects into an uncertainty of the reflectance. In order to maintain information about the correlation scales of the uncertainty effects, the uncertainties are

[3] Based on: Rüthrich, Frank, Viju O. John, Rob A. Roebeling, Ralf Quast, Yves Govaerts, Emma R. Woolliams and Jörg Schulz, 2019, Climate Data Records from Meteosat First Generation Part III: Recalibration and Uncertainty Tracing of the Visible Channel on Meteosat-2–7 Using Reconstructed, Spectrally Changing Response Functions, Remote Sens. 2019, 11(10), 1165; https://doi.org/10.3390/rs11101165

combined into two separate layers: an independent layer for uncorrelated effects and a structured layer for correlated effects.

Those uncertainty layers allow the proper quantification of the uncertainties resulting from, for example, the changing resolution of the dynamic range (6 bit to 8 bit), the different noise levels of the detectors, or the remaining uncertainties of the recalibration process. Moreover, they enable users to properly propagate the uncertainties into higher level products. An example of the reflectance and uncertainties from the FCDR for Algeria is provided as a time series in Figure 8. Note that the jumps between the instruments are expected due to the different shapes of the SRFs. Accordingly they are not a remainder of an incomplete calibration process.

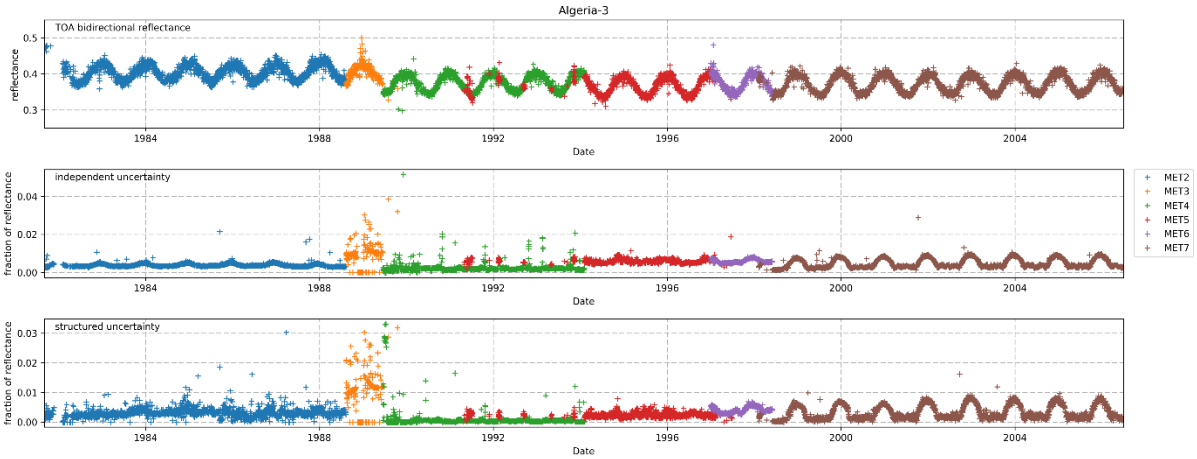

Figure 8: Recalibrated MVIRI clear sky reflectance time series and uncertainties for the Algeria-3 site, calibrated with the reconstructed, in-flight characterised SRF.

Not yet included in the uncertainty analysis of the FCDR is an uncertainty of the solar spectrum. As the same solar spectrum is used for the calibration and for the reflectance computation, the impact on the uncertainty budged is assumed to largely cancel out. However, a future release of the dataset should include a proper quantification of this effect. The same holds true for a revision of the assumption of entirely uncorrelated errors of the modelled atmosphere that is used for the vicarious calibration.

In a thorough validation against data from the SEVIRI instrument onboard MSG and against collocated and ray-matched measurements from SCIAMACHY the improved trueness of the dataset over cloudy and ocean areas has been demonstrated. Over cloudy areas, the harmonised MVIRI FCDR is brighter than the operational MVIRI data record, which results in a better match with the SEVIRI cloud reflectances. The brighter reflectance values for high-clouds, for example, are estimated to affect the top of atmosphere outgoing shortwave radiation by about 8 W/m2. The difference between the harmonised MVIRI FCDR and the operational MVIRI data record is small over areas with dominant spectral contributions in the green and red part of the spectrum. The analysis of SNOs between the harmonised MVIRI FCDR and SCIAMACHY has revealed excellent agreement with slopes close to unity (~0.98 over ocean areas and ~0.96 over land areas).

5 Microwave Radiometer FCDR

The scientific basis of the Microwave Humidity Sounder Fundamental Climate Data Record is reported thoroughly in the following peer-reviewed papers:

1. Paper describing the method to use the Moon as calibration standard:
   Burgdorf, M. J., S. A. Buehler, T. Lang, S. Michel, I. Hans, 2016: The Moon as a photometric calibration standard for microwave sensors, ATMOS MEAS TECH, 9, 3467-3475.
2. Paper describing the method to verify inter channel uniformity:
   Burgdorf, M., Hans, I., Prange, M., Lang, T., Buehler, S.A., 2018, Inter-channel uniformity of a microwave sounder in space, Atmospheric Measurement Techniques 11, 4005–4014.
3. Paper describing noise behavior of historic microwave instruments:
   Hans, I., Burgdorf, M., John, V. O., Mittaz, J., and Buehler, S. A.: Noise performance of microwave humidity sounders over their lifetime, Atmos. Meas. Tech., 10, 4927-4945, https://doi.org/10.5194/amt-10-4927-2017, 2017
4. Paper describing the quality of the FIDUCEO microwave FCDR:
   Hans, Imke, Martin Burgdorf, Stefan A. Buehler, Marc Prange, Theresa Lang and Viju O. John, 2019, An Uncertainty Quantified Fundamental Climate Data Record for Microwave Humidity Sounders, Remote Sens. 2019, 11(5), 548; https://doi.org/10.3390/rs11050548
5. Paper describing the quality of the FIDUCEO microwave FCDR:
   I. Hans, M. Burgdorf, S.A. Buehler, M. Prange, T. Lang and V.O. John, 2019, An Uncertainty Quantified Fundamental Climate Data Record for Microwave Humidity Sounders, Remote Sensing, 11(5), 548; https://doi.org/10.3390/rs11050548
6. Paper identifying radio frequency interference as main reason for biases of two microwave sounders: *I. Hans, M. Burgdorf, S.A. Buehler, 2019, Onboard radio frequency interference as the origin of inter-satellite biases for microwave humidity sounders, Remote Sensing, 11(7), 866; https://doi.org/10.3390/rs11070866*

The contents and conclusions of these papers are summarized in the following sections.

5.1 The Moon as a photometric calibration standard for microwave sensors[4]

Instruments on satellites for Earth observation on polar orbits usually employ a two-point calibration technique, in which deep space and an onboard calibration target provide two reference flux levels. As the direction of the deep-space view is in general close to the celestial equator, the Moon sometimes moves through the field of view and introduces an unwelcome additional signal. One can take advantage of this intrusion, however, by using the Moon as a third flux standard, and this has actually been done for checking the lifetime stability of sensors operating at visible wavelengths. As the disk-integrated thermal emission of the Moon is less well known than its reflected sunlight, this concept can in the microwave range only be used for stability checks and intercalibration. An estimate of the frequency of appearances of the Moon in the deep-space view, a description of the limiting factors of the measurement accuracy and models of the Moon's brightness, and a discussion of the benefits from complementing the naturally occurring appearances of the Moon with dedicated spacecraft maneuvers show that it would be possible to detect photometric lifetime drifts of a few percent with just two measurements. The pointing accuracy is the most crucial factor for the value of this method. Planning such observations in advance would be particularly beneficial, because it allows observing the Moon at well-defined phase angles and putting it at the center of the field of view. A constant phase angle eliminates the need for a model of the Moon's brightness when checking the stability of an instrument. With increasing spatial resolution of future microwave sensors another question arises, viz. to what extent foreground emission from objects other than the Moon will contaminate the flux entering the deep-space view, which is supposed to originate exclusively in the cosmic microwave background. We conclude that even the brightest discreet sources have flux densities below the detection limit of microwave sensors in a single scan.

With decreasing beamwidth at 183 GHz – 3.3◦ for SSM/T2, 1.1◦ for AMSU-B, and 0.65◦ for MWI – the signal of the Moon at its appearances in the deep-space view has increased relative to the contribution from the cosmic microwave background. As a consequence, it will be possible for future missions to measure the lunar flux with sufficient accuracy to check whether the requirements on the stability of the instrument are fulfilled.

While the emissivity of the Moon itself can confidently be assumed to be constant, it is essential to minimize the uncertainties related to the dependence of the flux on phase angle and the position of the Moon in the field of view. Both sources of error are best addressed with dedicated spacecraft maneuvers. If such maneuvers also include a raster map, one can characterize the beam pattern in flight. For this purpose, however, deconvolution of the images will become necessary, because the Moon is an extended source, especially for ICI and MWI. A raster map would also aid in determining the exact position of the Moon. If an accuracy of 1/10 of the 3 db bandwidth could be achieved, the corresponding flux error would amount to only a few percent. Its invariability makes the Moon also well suited for intercalibration between sensors that were operational at quite different epochs. This requires identical beam patterns of the sensors, an assumption that can be checked by means of the light curves themselves. Given the fact that the unplanned lunar intrusions in the deep-space view happen over a wide range of phase angles,

[4] Based on: Burgdorf, M. J., S. A. Buehler, T. Lang, S. Michel, I. Hans, 2016: The Moon as a photometric calibration standard for microwave sensors, ATMOS MEAS TECH, 9, 3467-3475.

because of orbital drifts and different viewing geometries, it is quite possible to find pairs of observations with similar phase angles from different satellites. This way one eliminates the unavoidable differences in scene temperature that adversely affect other methods like simultaneous nadir overpasses and zonal averages. A ground-based observing program of the Moon at the wavelengths of the window channels would considerably reduce the errors associated with remaining phase angle differences and libration. Microwave sensors in space, however, also operate at wavelengths for which the Earth's atmosphere is opaque. Furthermore, Zheng et al. (2012) showed that the brightness temperature of the warmest features on the lunar surface can vary by 30 K between different frequencies. Hence a complete model of the brightness of the Moon should allow for variations with frequency. Observations of the Moon carried out from an airplane flying in the stratosphere, e.g., ISMAR (International SubMillimeter Airborne Radiometer; Fox et al., 2014), would avoid 99 % of the water vapor in the Earth's atmosphere. Unfortunately, however, the Moon can only cover a small fraction of the beam of ISMAR, which has a halfpower width of some 5◦. Therefore ground-based millimeter observatories are a more promising alternative. They can easily resolve the lunar disk spatially, but obviously they cannot be used for observations of the Moon at 183.3 GHz. While the Moon produces thousands of counts when moving through the deep-space view, the possible impact from other discreet sources in the sky on the low-level reference flux from the cosmic microwave background is orders of magnitude smaller. Even with next-generation instruments, intrusions in the DSV from objects other than the Moon will have no significant impact on the calibration accuracy in the microwave range.

5.2 Inter-channel uniformity of a microwave sounder in space[5]

We analyzed intrusions of the Moon in the deep space view of the Advanced Microwave Sounding Unit-B on the NOAA-16 satellite and found no significant discrepancies in the signals from the different sounding channels between 2001 and 2008. However, earlier investigations had detected biases of up to 10 K, by using simultaneous nadir overpasses of NOAA-16 with other satellites. These discrepancies in the observations of Earth scenes cannot be due to non-linearity of the receiver or contamination of the deep space view without affecting the signal from the Moon as well. As neither major anomalies of the on-board calibration target nor the local oscillator were present, we consider radio frequency interference in combination with a strongly decreasing gain the most obvious reason for the degrading photometric stability. By means of the chosen example we demonstrate the usefulness of the Moon for investigations of the performance of microwave sounders in flight.

Intrusions of the Moon in the DSV can be used to obtain otherwise inaccessible information about the characteristics of microwave sounders in flight. This is because the Moon provides a third flux reference, in addition to the CMB and the OBCT, with a spectrum that closely resembles a black body. This property makes it particularly suited for checks of the uniformity of sounding channels, where vicarious calibration is not an option. Another characteristic of the Moon is that it fills only a fraction of the beams of past and present microwave sounders and therefore provides a flux level much lower than Earth scene and OBCT (see Fig. 3). As a consequence, the Moon becomes a unique diagnostic tool for checking the cold space temperature bias correction and, in case of insufficient or missing SNOs, non-linearity. Such characterization of instrumental effects is essential for calculating uncertainties and harmonization coefficients of fundamental climate data records, as undertaken in FIDUCEO.

In case of AMSU-B on NOAA-16 we found that the Moon signal from channel 20 agrees within 0.6 % with the average signal of channels 18 and 19. The following conclusions can be drawn.

The co-registration of the sounding channels is very good, and the beam solid angle of channel 20 is within 0.3 %, the same as the average beam solid angle of channels 18 and 19, else they could not have given the same value for a source much smaller than OBCT and DSV. This result was to be expected because of the common quasi-optic feed of all sounding channels with AMSU-B. However, the agreement among the sounding channels also proves that the Earth radiation entering the DSV pixels through the side lobes does not significantly alter the overall signal, because this radiation corresponds to different brightness temperatures in each channel. The scatter of the measured signal ratio can be fully explained by the uncertainties of the gain and the Gaussian fit.

We attribute the bias in the sounding channels of AMSU-B on NOAA-16 to a simple and well-known effect, namely radio frequency interference, by eliminating all other possible causes. Although this finding needs confirmation by a careful investigation of the interference in flight, we recommend excluding periods of active transmitters when calculating inter-calibration coefficients (Ferraro, 2015).

[5] Based on: Burgdorf, M., Hans, I., Prange, M., Lang, T., Buehler, S.A., 2018, Inter-channel uniformity of a microwave sounder in space, Atmospheric Measurement Techniques 11, 4005–4014.

One type of bias identified by Zou and Wang (2011) with AMSU-A, namely inaccurate calibration non-linearity, was ruled out in our investigation of AMSU-B. This finding provides evidence that the approach taken in the FIDUCEO project of harmonizing AMSU-B and MHS with the help of simultaneous nadir overpasses is sound, because the calculation of time-dependent nonlinear coefficients in flight, which would render that method impractical, is unnecessary.

Our characterization of sounding channels in flight demonstrates the potential of using intrusions of the Moon in the DSV as diagnostic tool for AMSU-B. Still higher accuracy is possible with MHS because of its lower NEΔT. As MHS is equipped with a sounding channel at 190.3 GHz with its own quasi-optic feed and local oscillator, the co-registration, bias correction, etc. will be less uniform among the channels, making their characterization even more important. In order to include also the window channels in the kind of analysis we presented, the differences of the brightness temperature of the Moon between the different radio wavebands must be known. A model describing them with the required accuracy is not available and remains therefore a worthwhile task for the future.

The Moon came 304 times closer than 0.1◦ to the centre of a DSV of MHS on NOAA-18 between launch and 1 June 2018. This large number opens up the possibility to use the Moon as a reference for identifying the long-term stability of microwave sounders. For this purpose it will be advantageous to identify and to process the relevant level 1b data automatically. The essential steps of such a procedure are as follows.

1. Identify the Moon intrusions: this will be easy if the lunar angles are known (Octets 1473–1480 in the MHS level 1b files). All events where the Moon did not come closer than 0.4◦ to one of the DSVs and closer than 1.2◦ to at least one other DSV should be rejected.
2. For each intrusion detected in the previous step, a Gaussian should be fitted to the number of counts as a function of scan number for each DSV and channel. This requires removing the baseline counts, i.e. those that would be present without the Moon, e.g. with a polynomial fit to the counts in the scans before and after the Moon intrusion.
3. If the height of these Gaussians is significantly different from zero for three DSVs of each channel, then another Gaussian should be fitted to their amplitudes as a function of DSV number.
4. Finally the gain has to be calculated for each channel from the baseline counts and the counts obtained when viewing the OBCT. The amplitude of the Gaussian fit from the previous step then has to be divided by the gain.
5. However, due to occasional anomalies in the data it will always be necessary to inspect the Gaussian fits for outliers in the “light curves” and proper baseline removal.

We conclude with a description of the potential of the Moon for in-orbit verification of future microwave imagers like MWI (MicroWave Imager). For the channels with a smaller beam that are planned for these facilities, the method we described in this paper cannot be applied the same way, as the light curve will no longer have the shape of a Gaussian. This is because the finite size of the Moon and the asymmetric temperature distribution of its surface will become more relevant. A specially defined scan profile – in the ideal case a two-dimensional raster map with a step size of 0.1◦ as proposed by Bonsignori (2018) – will then be advantageous. It will enable measurements of the Moon's flux with much better signal-to-noise ratio, because it will fill a larger part of the beam, and it will provide several additional reference flux levels, because one can point at regions of the Moon with quite different temperatures. This way the non-linearity, to give just one example, can be characterized over a large flux range.

5.3 Noise performance of microwave humidity sounders over their lifetime[6]

The microwave humidity sounders Special Sensor Microwave Water Vapor Profiler (SSMT-2), Advanced Microwave Sounding Unit-B (AMSU-B) and Microwave Humidity Sounder (MHS) to date have been providing data records for 25 years. So far, the data records lack uncertainty information essential for constructing consistent long time data series. In this study, we assess the quality of the recorded data with respect to the uncertainty caused by noise. We calculate the noise on the raw calibration counts from the deep space views (DSVs) of the instrument and the noise equivalent differential temperature (NEΔT) as a measure for the radiometer sensitivity. For this purpose, we use the Allan deviation that is not biased from an underlying varying mean of the data and that has been suggested only recently for application in atmospheric remote sensing. Moreover, we use the bias function related to the Allan deviation to infer the underlying spectrum of the noise. As examples, we investigate the noise spectrum in flight for some instruments. For the assessment of the noise evolution in time, we provide a descriptive and graphical overview of the calculated NEΔT over the life span of each instrument and channel. This overview can serve as an easily accessible information for users interested in the noise performance of a specific instrument, channel and time. Within the time evolution of the noise, we identify periods of instrumental degradation, which manifest themselves in an increasing NEΔT, and periods of erratic behaviour, which show sudden increases of NEΔT interrupting the overall smooth evolution of the noise. From this assessment and subsequent exclusion of the aforementioned periods, we present a chart showing available data records with NEΔT < 1K. Due to overlapping life spans of the instruments, these reduced data records still cover without gaps the time since 1994 and may therefore serve as a first step for constructing long time series. Our method for count noise estimation, that has been used in this study, will be used in the data processing to provide input values for the uncertainty propagation in the generation of a new set of Fundamental Climate Data Records (FCDRs) that are currently produced in the project Fidelity and Uncertainty in Climate data records from Earth Observation (FIDUCEO).

The results provide users with information on the uncertainty due to noise that they should expect when using the data sets of the microwave sounders SSMT-2, AMSUB and MHS. The chart in Fig. 9 reveals the possibility to concatenate the available data for constructing gap-less long time series since 1994 at a noise level below 1 K for all frequency intervals that the instruments cover. This is of major interest for climate researchers who need long time series with low noise levels in order to investigate possible trends. Apart from the stand-alone results as information content for users of these microwave sounders' data, our analysis is of direct use for the FIDUCEO project: the method for estimating the count noise for the DSV and OBCT will be used in the processing of level 1b to level 1c FIDUCEO FCDR in order to provide on-the-fly input values for the uncertainty propagation. This FCDR will provide a field-of-viewwise estimate of uncertainty in brightness temperature due to count noise for every scan line and orbit. Additionally, the FCDR will contain extensive information that will further close the gap of lacking information on uncertainty.

[6] Based on: Hans, I., Burgdorf, M., John, V. O., Mittaz, J., and Buehler, S. A.: Noise performance of microwave humidity sounders over their lifetime, Atmos. Meas. Tech., 10, 4927-4945, https://doi.org/10.5194/amt-10-4927-2017, 2017

5.4 An Uncertainty Quantified Fundamental Climate Data Record for Microwave Humidity Sounders[7]

To date, there is no long-term, stable, and uncertainty-quantified dataset of upper tropospheric humidity (UTH) that can be used for climate research. As intermediate step towards the overall goal of constructing such a climate data record (CDR) of UTH, we produced a new fundamental climate data record (FCDR) on the level of brightness temperature for microwave humidity sounders that will serve as basis for the CDR of UTH. Based on metrological principles, we constructed and implemented the measurement equation and the uncertainty propagation in the processing chain for the microwave humidity sounders. We reprocessed the level 1b data to obtain newly calibrated uncertainty quantified level 1c data in brightness temperature. Three aspects set apart this FCDR from previous attempts: (1) the data come in a ready-to-use NetCDF format; (2) the dataset provides extensive uncertainty information taking into account the different correlation behaviour of the underlying errors; and (3) inter-satellite biases have been understood and reduced by an improved calibration. Providing a detailed uncertainty budget on these data, this new FCDR provides valuable information for a climate scientist and also for the construction of the CDR.

Our new FCDR for microwave humidity sounders addresses three problems of operational data that we intended to solve to make the data usable for climate research.

First, we facilitate the handling of the data by providing the FCDR in ready-to-use NetCDF files. Each of these files covers one orbit reaching from one equator and crossing to the next in the same flight direction. This equator-to-equator frame removes all doubled data and hence prevents the appearance of corresponding sampling artefacts. The FCDR contains concise quality information on pixel level and maintains the traceability back to the original level 1b data.

Second, the FCDR provides extensive pixel-level uncertainty information, considering the correlation behaviour of the underlying errors.

Third, we have strong evidence that we understood the origin of the most important inter-satellite biases. By applying corresponding corrections, we were able to produce an FCDR for MW sounders of distinctly improved consistency. The sounding channels show very good agreement between the instruments and offer the possibility for using the FCDR for the production of the higher level CDR.

[7] Based on: Hans, Imke, Martin Burgdorf, Stefan A. Buehler, Marc Prange, Theresa Lang and Viju O. John, 2019, An Uncertainty Quantified Fundamental Climate Data Record for Microwave Humidity Sounders, Remote Sens. 2019, 11(5), 548; https://doi.org/10.3390/rs11050548

5.5 Disk-Integrated Lunar Brightness Temperatures between 89 and 190 GHz[8]

Following the recommendation of project advisor, R. Ferraro, at the FIDUCEO project General Assembly meeting in February 2018 to use Moon intrusions for calibration, UHAM investigated, whether existing models of the disk-integrated lunar brightness temperature are accurate enough for this purpose. A re-calibration of different instruments based on observations of the Moon would avoid several problems of the standard harmonization procedure, e. g. with the match-ups between different instruments or the choice of the right reference instrument. The main problem with the Moon is that the dependence of its brightness temperature from the phase angle has to be known with high accuracy.

Hence measurements of the disk-integrated brightness temperature of the Moon at 89, 157, 183, and 190 GHz were carried out for phase angles between -80° and 50° relative to full Moon. They were obtained with the Microwave Humidity Sounder (MHS) on NOAA-18 from 39 instances when the Moon appeared in the deep space view of the instrument. Polynomials were fitted to the measured values and the maximum temperature and the phase angles of its occurrence were determined.

This investigation has produced two major, new findings:

1. The phase angle of the Moon, where the disk-integrated brightness temperature reaches its maximum, is at the lower frequencies larger than each of the models predicted, therefore they do not reproduce the difference between waxing and waning Moon correctly (see Figure 6).
2. The difference in beam size between the sounding channels and the channel H2 is almost ten times as large as the value measured with the ground tests that were supposed to demonstrate the compliance with the requirements for MHS on NOAA-18. This finding was possible, because the calculated lunar radiances depend strongly on the fraction of the beam that is covered by the Moon.

[8] Based on: *M.J. Burgdorf, S.A. Buehler, I. Hans, M. Prange, 2019, Disk-Integrated Lunar Brightness Temperatures between 89 and 190 GHz, Advances in Astronomy; https://doi.org/10.1155/2019/2350476.*

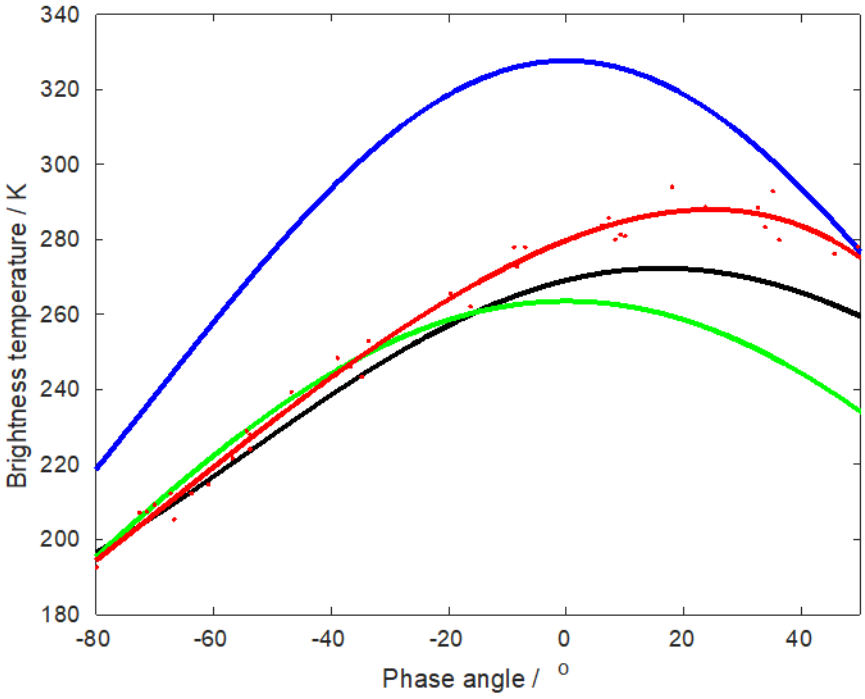

Figure 6: Disk-integrated brightness temperature of the Moon for different phase angles relative to full Moon at 89 GHz. Blue: Equation 4 in Mo and Kigawa (2007), green: Equation 4 and Table II in Yang et al. (2018), black: Keihm (1984, numbers from web page and personal communication), red: MHS on NOAA-18, single measurements (dots) fitted with polynomial of order five.

On top of that, our investigation demonstrated that precise measurements from weather satellites can provide useful information also about objects other than Earth. It also underlined the relevance of the Moon for cross calibration, because the Moon enables the detection of biases between quite different instruments operating at quite different times, a weighty prerequisite for studies of climate change with satellite data.

A new model of the lunar brightness temperature is needed that reflects correctly the time delay between full Moon and maximum brightness temperature as determined with weather satellites. The current uncertainty of the phase lag can be further reduced by analyzing more than the 39 intrusions of the Moon in the DSV that were the basis of the results presented by us. The Moon appeared altogether 1566 times in the DSV of MHS on NOAA-18 between May 2005 and October 2018, and this number is similar for other satellites. The uncertainty of the maximum brightness temperature of the Moon can be reduced by analyzing data from more satellites: there are five MHSs and three AMSU-Bs in orbit, and averaging their measurements would significantly mitigate the impact of systematic errors.

A similar method, mutatis mutandis, could be used to establish the Moon as calibration reference in the thermal infrared.

5.6 Onboard Radio Frequency Interference as the Origin of Inter-Satellite Biases for Microwave Humidity Sounders[9]

To understand the causes of inter-satellite biases in climate data records from observations of the Earth (which is crucial for constructing a consistent time series of the essential climate variables) we analyze the strong scan- and time-dependent biases observed for the microwave humidity sounders on board the NOAA-16 and NOAA-19 satellites. We find compelling evidence that radio frequency interference (RFI) is the cause of the biases. We also devise a correction scheme for the raw count signals for the instruments to mitigate the effect of RFI. Our results show that the RFI-corrected, recalibrated data exhibit distinctly reduced biases and provide consistent time series.
Analyzing inter-satellite biases using global monthly means, we found that a risk of RFI impact exists and may cause biases even if it was not detectable in the verification phase of the instrument. Large biases may emerge from this in the later years of the mission if the gain decreases. Taking the example of NOAA-16 and NOAA-19, we found strong evidence that RFI is the origin for the observed inter-satellite biases compared to NOAA-18. Hence, we found a plausible explanation for these known biases.
Moreover, we provided a correction scheme to mitigate the effects of RFI. This correction scheme operates on the raw Earth counts and corrects these before they enter the calibration procedure. By recalibrating the data for the example instruments on NOAA-16 and NOAA-19, we gained a distinct improvement in terms of the consistency and stability of the brightness temperature time series.

[9] Based on: *I. Hans, M. Burgdorf, S.A. Buehler, 2019, Onboard radio frequency interference as the origin of inter-satellite biases for microwave humidity sounders, Remote Sensing, 11(7), 866; https://doi.org/10.3390/rs11070866.*

6 High-resolution Infrared Sounder (HIRS) FCDR

Much of the scientific basis of the HIRS FCDR is based on the following peer reviewed paper:

1. Paper describing the method to calculate coviariances of the channels of the HIRS instrument: *Holl, Gerrit, Jonathan P. D. Mittaz, Christopher J. Merchant, 2019, Error covariances in High-resolution Infrared Radiation Sounder (HIRS) radiances, Remote Sensing, 11 (11). 1337. ISSN 2072-4292 doi: https://doi.org/10.3390/rs11111337*

Additional description of the scientific basis is included in the following sections.

6.1 Error covariances in High-resolution Infrared Radiation Sounder (HIRS) radiances [10]

The High-resolution Infrared Radiation Sounder (HIRS) has been flown on 17 polar-orbiting satellites between the late 1970s and the present day. HIRS applications require accurate characterisation of uncertainties and inter-channel error correlations, which has so far been lacking. Here, we calculate error correlation matrices by accumulating count deviations for sequential sets of calibration measurements, and then correlating deviations between channels (for a fixed view) or views (for a fixed channel). The inter-channel error covariance is usually assumed to be diagonal, but we show that large error correlations, both positive and negative, exist between channels and between views close in time. We show that correlated error exists for all HIRS and that the degree of correlation varies markedly on both short and long timescales. Error correlations in excess of 0.5 are not unusual. Correlations between calibration observations taken sequentially in time arise from periodic error affecting both calibration and Earth counts. A Fourier spectral analysis shows that, for some HIRS instruments, this instrumental effect dominates at some or all spatial frequencies. These findings are significant for application of HIRS data in various applications, and related information will be made available as part of an upcoming Fundamental Climate Data Record covering all HIRS channels and satellites.

The observed phenomena can broadly be classified into two categories that may or may not be related: error correlations between channels, and periodic error. In some cases, we see both, in other cases only one of those, in yet other cases neither. It is difficult to determine the physical origins of the observed behaviour purely from in-flight data. The diversity of the observed behaviour across different satellites and channels suggests multiple physical causes may be relevant to various members of the HIRS series.

Retrievals of geophysical variables often involve a characterisation of error correlations between measurement vectors, or explicit or implicit assumptions about such error correlations [Rodgers et al. (2000)]. Typically, instrument errors are assumed to be uncorrelated between channels. Cross-channel error correlation reduces the information content of multi-channel observations, and can be expected to degrade the quality of atmospheric soundings derived from HIRS data where they are present. Moreover, performing a retrieval with the wrong a priori covariance matrix will lead to a retrieval with an incorrect a posteriori covariance matrix. Future work will quantify such implications. Where the periodic error is adequately predictable, it may be possible to correct for it (leaving some residual errors). Since there are space, IWCT, and possibly ICCT views every 40 scanlines, a correction model could be frequently updated. This may enhance significantly the

[10] Based on: Holl, Gerrit, Jonathan P. D. Mittaz, Christopher J. Merchant, 2019, Error covariances in High-resolution Infrared Radiation Sounder (HIRS) radiances. , Remote Sens. (accepted)

utility of HIRS data in situations where such correlated error affects Earth views. Such a correction is recommended for future work.
HIRS has the potential for long-term climate studies, but only with metrologically traceable uncertainties and sensor-to-sensor harmonisation, including correlation information such as presented in this study.

6.2 Summary of HIRS Uncertainty & Cross-channel Correlation

For the development of an FCDR, the measurement function is that which converts raw data (e.g. measured counts and calibration target values) into the FCDR quantity (e.g. radiance or reflectance). In almost all cases, the input effects are metrologically independent (they have no common error) and the propagation of uncertainty requires only information on the magnitude of the uncertainty associated with each effect and the sensitivity coefficient that converts the uncertainty in that effect into the uncertainty associated with the FCDR measurand (e.g. radiance).
For the development of a CDR, however, the measurement function often takes as input FCDR values from different spectral bands, along with additional inputs relating to the model used. This means that we require an understanding of the error covariance between the FCDR quantities as measured in different spectral bands. Furthermore gridded, filled or smoothed products the measurement function combines data from different spatial pixels. We therefore need an understanding of the error covariance between the FCDR quantities as measured in different pixels of an image.
To account for this, the full FCDR development in FIDUCEO has included an analysis of the error correlation structure across spectral bands and across space (from pixel to pixel within a scanline and from scanline to scanline within an orbit/image). Information about this process is given in the D2-2 reports.
To investigate error correlations between channels or views, specific sets of calibration measurements are analysed, directly visualising space or IWCT counts. Estimations of error correlation matrices between channels and between views are also calculated, whilst Fourier transforms over time are calculated to quantify to what degree the signal is polluted by periodic error. Periodic error in this case is defined to mean any unwanted component of the measurement that is oscillating, sinusoidal, or otherwise (quasi-)periodic in time.
Deviations are calculated within the 48 space or IWCT views. Several thousand sets of calibration measurements are retrieved, and Pearson correlation coefficents and correlation coefficents are calculated for correlations with each channel and with each view.

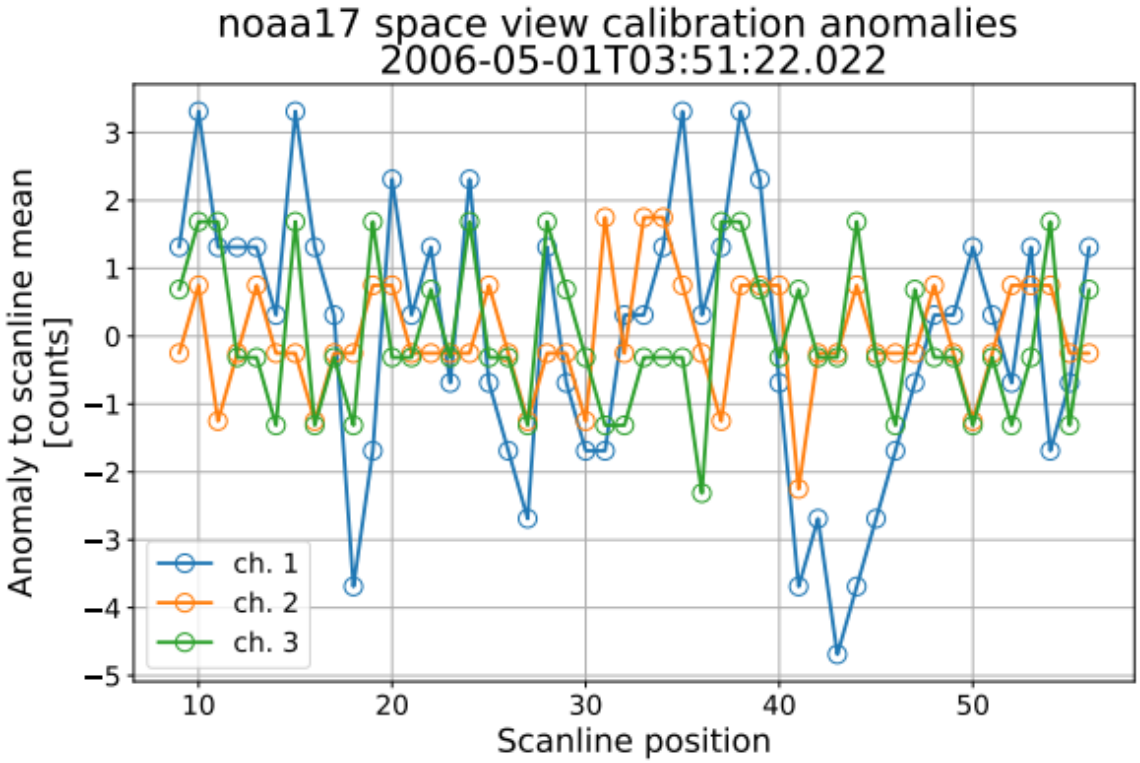

Figure 6.2.1 - Example of space view deviations for one set of calibration measurements for channels 6–8 on NOAA-14. The date and time for the measurements are shown in the figure title.

If HIRS were operating as intended, it would expected that space view and IWCT view deviations would be independent between channels and between views. In reality, space view count deviations may be uncorrelated (as expected), exhibit strong positive correlation, or even exhibit significant negative correlation. For example, Figure 6.2.1 shows a case where space view correlations are absent, showing deviations for channels 6–8 for a single set of calibration measurements on NOAA-14. In contrast, Figure 6.2.2 shows an example of strong positive space view count deviations, in this case for channels 13–15 for three sets of calibration measurements on NOAA-15. Two features are immediately apparent from the figure: firstly, the deviations for the three channels are very highly correlated. Therefore, the deviations cannot be caused by white noise, but must be dominated by a shared physical mechanism. Since the measurements for different channels are not taken simultaneously, that mechanism must have some temporal persistence. Given the features displayed, the source of the deviation must have a period of around 0.5 s. Further examples exist where channel anomalies are in phase, or in some cases, are synced perfectly out of phase, with each other across satellites, indicating further temporal errors. A full table of these can be found in the above paper.

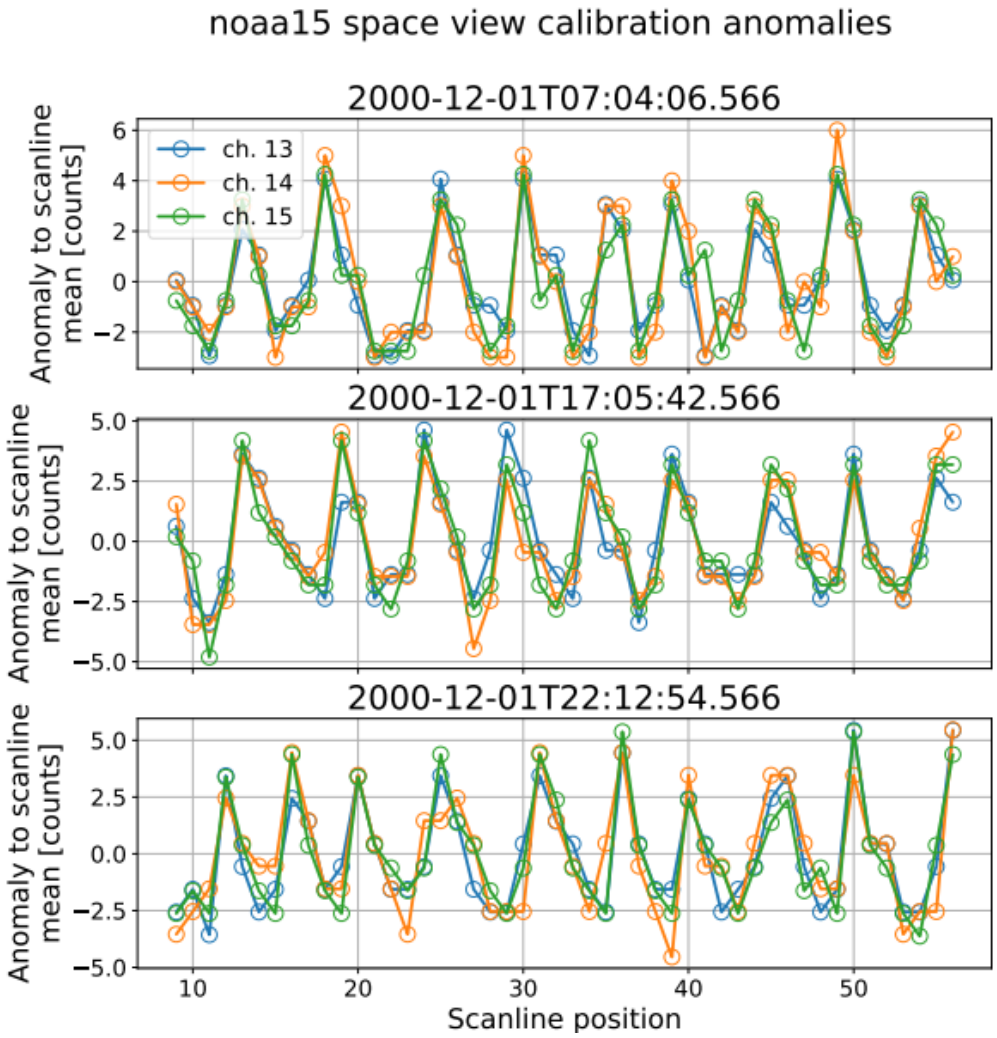

Figure 6.2.2 - Like Figure 6.2.1, but showing three examples for channels 13–15 on NOAA-15

To take a closer look at such periodicities, the correlations between different space view anomalies are calculated for both the early and late periods for each satellite. These can be shown in matrix form, with the periodicity clear from the striped pattern. Lack of striping, as evident on noaa 18, does not necessarily mean there is no periodic error, but that the period error may shift in phase, averaging out over the matrix averaging period. By finally calculating the power spectra for space, IWCT, and Earth views, we can compare the magnitude of the periodic error to the magnitude of natural variability in the Earth atmosphere, and determine if the Earth views should be expected to be significantly affected by periodic error. All satellites are shown to follow a power law distribution with a negative slope, meaning that the variability between two earth pixels is larger as distance increases. For most users of HIRS data, the most important situation is when the power of the IWCT and space error—which is completely instrumental—approaches or exceeds the power of the signal from the Earth views. This may either happen when the data have dominant white noise, or when a strong periodic effect is present in both calibration and Earth views. Cases of periodic errors which may affect Earth views are found across all satellites, as outlined in section 3.4 of Holl et al.

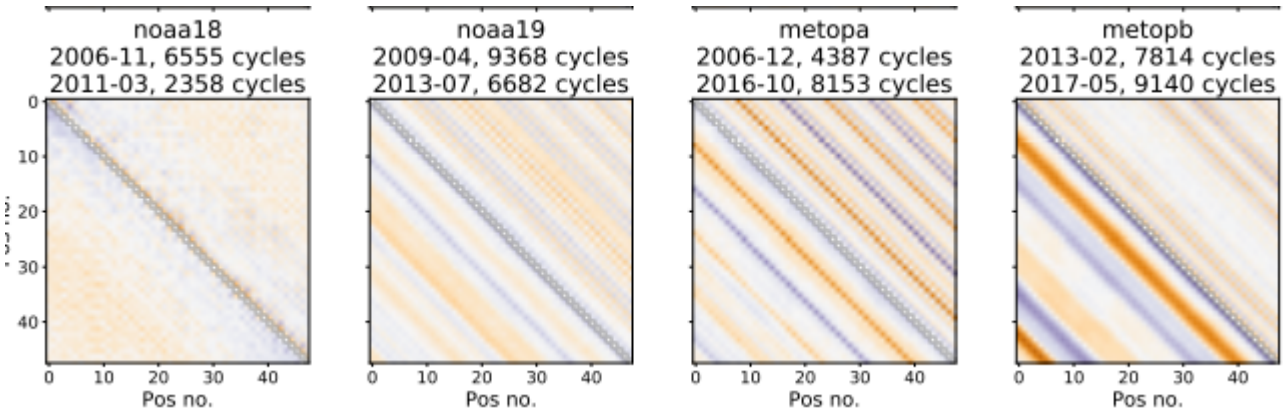

Figure 6.2.3 - Pearson product-moment correlation between the error at different views within a set of calibration measurements (labelled "pos no"), channel 9, for the IWCT view. The lower triangle refers to a month early in the lifetime of each instrument, whereas the upper triangle refers to a month late in its lifetime, each indicated in the title above each panel.

6.3 Self-emission model

As HIRS is not cooled, the contamination of retrievals via satellite self-emissions must be accounted for produce accurate retrievals. As the satellite moves around an orbit, it enters and exits through periods of night and day, causing fluctuations in this temperature, and thus fluctuations in the correction required due to self emission. Although this is corrected for by the calibration, those calibrations are too infrequent and a model is needed to estimate self-emission between the calibrations.

Self-emission in the HIRS FCDR is approximated as shown in the equation below.

$$L_{\text{self},y} = \sum_i k_i T_i^4 + 0 \,. \qquad \text{Eq 6-1}$$

where i refers to different temperatures, currently the baseplate, internal warm calibration target, scanmirror, scanmotor, and secondary telescope. The coefficients are trained using linear regression in a moving 24-hour window and updated every 6 hours.

Whilst this equation is suitable for determining the uncertainty over long time scales, it is considered that the linear approach, compared to a modelled environment approach which incorporates the temperature, emissivity, and solid angle, for all components directly visible by the detector, something which is not currently available.

This approach to self emission does lead to some problems, which can be seen within the FCDR. Firstly, as a linear approach is taken, the error in the uncertainty calculated peaks during scanlines furthest away from calibration points. Secondly, the linear regression model is only bound at one end, meaning that sudden jumps in the uncertainty are observed. These can propagate through to the brightness temperatures reported, and as can be seen in the channel 1 orbital maps in the HIRS D4.4, these can cause banding effects of the data. The effect can also be seen to be responsible for similar patterns in the independent uncertainty.

The self-emission technique is a step forward compared to current operational methods, but does not represent a complete metrological solution to this source of error.

6.4 HIRS Harmonisation

The principles of section 3.4 apply to HIRS harmonisation.

The HIRS FCDR is to be considered a harmonised (not homogenised) data record, meaning that the calibration methods used takes into account the sensors unique spectral response function. In this case, HIRS is harmonised throughout, and anchored to the IASI satellite retrievals through comparisons to MetOp-A for all channels. Harmonisation has been attempted for all channels and across all satellites. A variety of reasons (lack of suitable overlapping data, instrument failings, and bad data) prevent complete harmonisation across all channels and satellites from being possible using the developed methodology. Even so, for most channels, harmonisation of the HIRS product has shown a significant improvement in the continuous nature of the FCDR.
As figure 6.4.1 shows, harmonised data can be used to ensure that continuous records are produced. The spectral response functions for this 13.4 um channel well matched across the sensors, and so the observed brightness temperature after harmonisation shows (as is expected in this circumstance) good agreement between different satellites when times overlap.

from HIRS at 13.4 um (Channel 7)

FIDUCEO product, which although corrected for several errors, was a pre-harmonisation version. Whilst the retrievals from each individual sensor look continuous, there are clear jumps between sensors retrieving at the same time. There is both a large step in radiance between noaa 14 and 15, whilst there is a spread in radiances among the different satellites from 2005 onwards. When converted in brightness temperature and reflectances, these can be different by several K. For this channel, spectral responses are not as consistent, and some differences are expected – but the discrepancies here are larger than spectral responses differences would cause, pointing to inconsistencies in (unharmonized) calibration.

sensors. For this reason, harmonisation can be pursued as far back as late 1984 – beyond that the chain is broken.

Figure 6.4.2 – Averaged radiance from all satellites for HIRS Channel 4 from the pre-beta product, which did not have harmonisation applied.

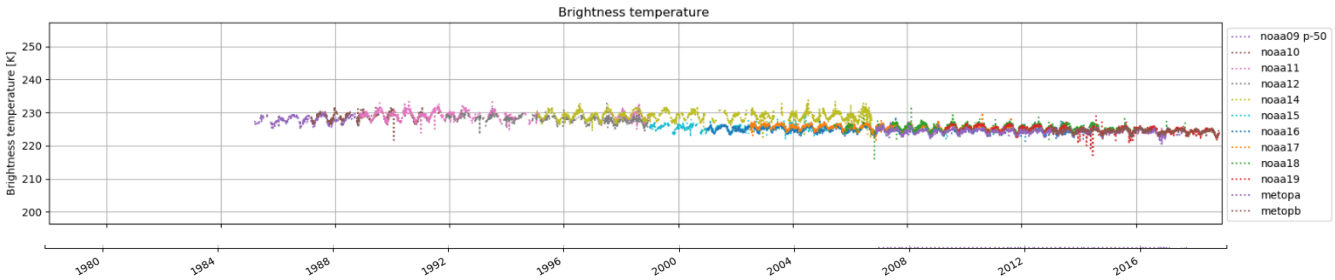

Figure 6.4.3 – Harmonised median retrieved Brightness temperature for all HIRS channel 4 sensors.

The post-harmonisation result is shown in Figure 6.4.3. Several unexpected discrepancies seen in the late 2000's have been removed due to the harmonisation process. An obvious step remains between HIRS on NOAA-14 and earlier, and those from NOAA-15 afterwards in (channel 4). This persists after harmonisation is applied, and we consider that this is likely due to systematic differences in spectral response function or instrument behaviour of the HIRS1 and HIRS2 sensors onboard satellites prior to NOAA 15, and the HIRS3 sensor onboard NOAA-15 and after. The harmonisation process considers the difference in spectral response function, and accounts for this in harmonising time series, meaning that whilst noaa 14 and noaa 15 retrieve brightness temperatures which are several K different, when corrected for spectral response function differences, the difference in brightness temperature is mostly removed.
An extreme illustration of the expected effects of spectral response effects is present in for channel 10, shown in figure 6.4.4. HIRS 1 and HIRS 2 sensors measured at 8.6 um, whilst from HIRS 2i and HIRS 3 and beyond the channel shifted to 12.3 um. The harmonisation process has, in this case, determined the harmonisation of NOAA 09 and 10, which both retrieve at 8.6 um, and shows a difference of around 40K compared to NOAA 11, which uses HIRS 2i and so retrieves at 12.3 um. NOAA 12 also retrieves at 8.6 um, but has no cross-over with NOAA 09 and 10, and so is not harmonised with them. This accounts for the differences seen between all satellites retrieving at 12.3 um, and the differences between NOAA 12 and the combined NOAA 09/10 retrieval sets.

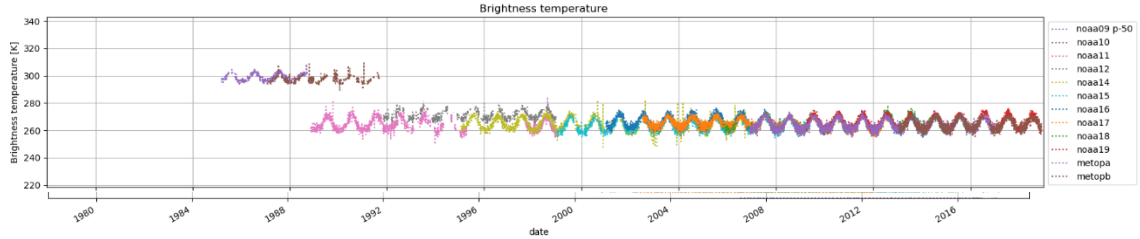

Figure 6.4.4 – Channel 10 median Brightness Temperature retrievals from all HIRS sensors.

Overall, the harmonisation has improved the consistency and stability of the FCDR dataset, and with the exception of highlighted cases, should lead to improved level 2 dataset production, which will allow for comparison to other datasets which have long time series. We believe that the harmonisation will show significant improvements in comparisons between such datasets and HIRS-produced data, especially at satellite crossovers and near the end of satellite lifetime.
The harmonised dataset has not solved all issues, but the advances it incorporates provide a good basis and new directions for future work in improving the HIRS FCDR. Work on the correlation of

the uncertainties, harmonisation and self-emission model have demonstrated significant progress and value that should be carried forward into future dataset production.

7 AVHRR FCDR

The scientific basis of the AVHRR FCDR uncertainty estimation is reported in the following peer reviewed paper:

1. Paper describing the method applied to derive uncertainties of the AVHRR FCDR:
   Mittaz, Jonathan, Christopher J Merchant, and Emma R Woolliams, 2019, Applying principles of metrology to historical Earth observations from satellite, Metrologia, Volume 56, Number 3

A simulation-based estimate for the error distribution of clear-sky infra-red brightness temperature was developed in order to understand the uncertainty for AVHRR. Calibration uncertainty and digitisation are found to dominate (Fig. 7.1.1).

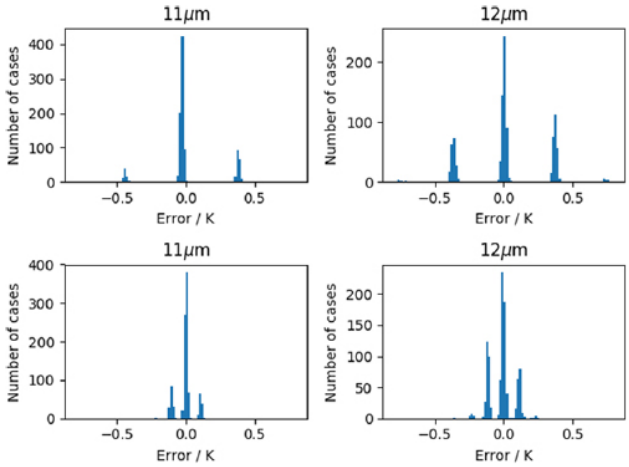

Figure 7.1 Traceable, simulated error distributions in AVHRR BTs. Top panels: scene temperature 200 K; bottom panels 300 K. Left panels: 11 μm channel; right panels: 12 μm channel.

The propagation of these errors to sea surface temperature causes highly non-Gaussian error distributions, a new insight illustrating the relevance of the approach to derivation of EO-based climate datasets.

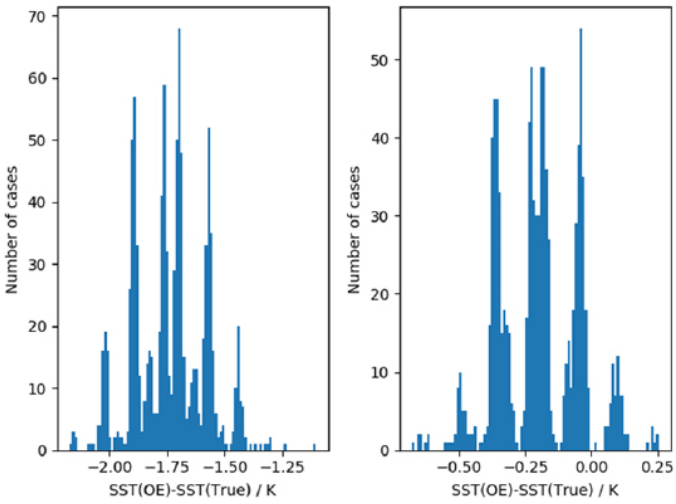

Figure 7.2 Distribution of the OE retrieval error for two examples of OE retrievals. The distributions are based on 1000 Monte-Carlo simulations where the input noise is from the instrument only.

Harmonisation of the AVHRR FCDR follows the principles of section 3.4, and results are presented in the metrological assessment of the FCDR.

8 References

FIDUCEO_Product User Guide – MVIRI FCDR Release 1.0, H2020 FIDUCEO, Issue 1, 1 September 2019.

FIDUCEO_Product User Guide – MHS FCDR Release 4.1, H2020 FIDUCEO, Issue 1, 29 January 2019.

FIDUCEO_Product User Guide – HIRS FCDR Beta Release 0.2, H2020 FIDUCEO, Issue 1, 14 June 2018.

FIDUCEO_Product User Guide – AVHRR FCDR Beta Release 0.1, H2020 FIDUCEO, Issue 1, 15 January 2019.

Block, T., Embacher, S., Merchant, C. J. and Donlon, C. (2018) *High performance software framework for the calculation of satellite-to-satellite data matchups (MMS version 1.2).* Geoscientific Model Development, 11 (6). pp. 2419-2427. ISSN 1991-9603

Burgdorf, M. J., S. A. Buehler, T. Lang, S. Michel, I. Hans, 2016: The Moon as a photometric calibration standard for microwave sensors, ATMOS MEAS TECH, 9, 3467-3475.

Burgdorf, M., Hans, I., Prange, M., Lang, T., Buehler, S.A., 2018, Inter-channel uniformity of a microwave sounder in space, Atmospheric Measurement Techniques 11, 4005–4014.

Chen, W.; Zhao, H.; Li, Z.; Jing, X.; Yan, L. Uncertainty Evaluation of an In-Flight Absolute Radiometric Calibration Using a Statistical Monte Carlo Method. IEEE Trans. Geosci. Remote Sens. 2015, 53, 2925–2934.

Chen, N.; Helder, D.; Angal, A.; Choi, J.; Xiong, X. Absolute Calibration of Optical Satellite Sensors Using Libya 4 Pseudo Invariant Calibration Site. Remote Sens. 2014, 6, 1327–1346.

Decoster, I.; Clerbaux, N.; Baudrez, E.; Dewitte, S.; Ipe, A.; Nevens, S.; Velazques Blazquez, A.; Cornelis, J. A spectral aging model for the Meteosat-7 visible band. *J. Atmos. Ocean. Technol.* **2013**, *30*, 496–509. [CrossRef]
Decoster, I.; Clerbaux, N.; Govaerts, Y.M.; Baudrez, E.; Ipe, A.; Dewitte, S.; Nevens, S.; Velazquez Blazquez, A.; Cornelis, J. Evidence of pre-launch characterization problem of Meteosat-7 visible spectral response. *Remote Sens. Lett.* **2013**, *4*, 1008–1017. [CrossRef]
Decoster, I.; Clerbaux, N.; Baudrez, E.; Dewitte, S.; Ipe, A.; Nevens, S.; Velazques Blazquez, A.; Cornelis, J. Spectral aging model applied to Meteosat First Generation visible band. *Remote Sens.* **2014**, *6*, 2534–2571. [CrossRef]
Giering, Ralf, Ralf Quast, Jonathan P. D. Mittaz, Samuel E. Hunt, Peter M. Harris, Emma R. Woolliams and Christopher J. Merchant, 2019, A Novel Framework to Harmonise Satellite Data Series for Climate Applications, Remote Sens. 2019, 11(9), 1002; https://doi.org/10.3390/rs11091002

Newey, W.K. Flexible simulated moment estimation of nonlinear errors-in-variables models. *Rev. Econ. Stat.* **2001**, *83*, 616–627. [CrossRef]
Harris, P.M.; Hunt, S.E.; Quast, R.; Giering, R.; Mittaz, J.P.D.; Woolliams, E.R.; Dilo, A.; Cox, M. Solving large structured non-linear least-squares problems with an application in Earth observation. in preparation.
Govaerts, Y.M. Correction of the Meteosat-5 and -6 radiometer solar channel spectral response with the Meteosat-7 sensor spectral characteristics. *Int. J. Remote Sens.* **1999**, *20*, 3677–3682. [CrossRef]
Govaerts, Y.M.; Clerici, M.; Clerbaux, N. Operational calibration of the Meteosat radiometer VIS band. *IEEE Trans. Geosci. Remote Sens.* **2004**, *42*, 1900–1914. [CrossRef]

Govaerts, Yves M., Frank Rüthrich, Viju O. John and Ralf Quast, 2019, Climate Data Records from Meteosat First Generation Part I: Simulation of Accurate Top-of-Atmosphere Spectral Radiance over Pseudo-Invariant Calibration Sites for the Retrieval of the In-Flight Visible Spectral Response, Remote Sens. 2018, 10(12), 1959; https://doi.org/10.3390/rs10121959

Hans, I., Burgdorf, M., John, V. O., Mittaz, J., and Buehler, S. A.: Noise performance of microwave humidity sounders over their lifetime, Atmos. Meas. Tech., 10, 4927-4945, https://doi.org/10.5194/amt-10-4927-2017, 2017

Hans, Imke, Martin Burgdorf, Stefan A. Buehler, Marc Prange, Theresa Lang and Viju O. John, 2019, An Uncertainty Quantified Fundamental Climate Data Record for Microwave Humidity Sounders, Remote Sens. 2019, 11(5), 548; https://doi.org/10.3390/rs11050548

Holl, Gerrit, Jonathan P. D. Mittaz, Christopher J. Merchant, 2019, Error covariances in High-resolution Infrared Radiation Sounder (HIRS) radiances. , Remote Sens. (accepted)

Merchant, Christopher J., Gerrit Holl, Jonathan P. D. Mittaz and Emma R. Woolliams, 2019, Radiance Uncertainty Characterisation to Facilitate Climate Data Record Creation, Remote Sens. 2019, 11(5), 474; https://doi.org/10.3390/rs11050474

Mittaz, Jonathan, Christopher J Merchant, and Emma R Woolliams, 2019, Applying principles of metrology to historical Earth observations from satellite, Metrologia, Volume 56, Number 3

Rodgers, C.D., Ed. Inverse Methods for Atmospheric Sounding: Theory and Practice; World Scientific Publishing: 2000; ISBN 10981022740X.

Rüthrich, F.; John, V.O.; Roebeling, R.A.; Quast, R.; Govaerts, Y.; Woolliams, E.R.; Schulz, J. Climate Data Records from Meteosat First Generation Part III: Recalibration and Uncertainty Tracing of the Visible Channel on Meteosat-2–7 Using Reconstructed, Spectrally Changing Response Functions. *Remote Sens.* **2019**, *11*, 1165. https://doi.org/10.3390/rs11101165 [CrossRef]
Quast, Ralf, Ralf Giering, Yves Govaerts, Frank Rüthrich and Rob Roebeling, 2019, Climate Data Records from Meteosat First Generation Part II: Retrieval of the In-Flight Visible Spectral Response, Remote Sens. 2019, 11(5), 480; https://doi.org/10.3390/rs11050480 [CrossRef]

Sterckx, S.; Livens, S.; Adriaensen, S. Rayleigh, Deep Convective Clouds, and Cross-Sensor Desert Vicarious Calibration Validation for the PROBA-V Mission. IEEE Trans. Geosci. Remote Sens. 2013, 51, 1437–1452.

Tarantola, A. *Inverse Problem Theory and Methods for Model Parameter Estimation*; Society for Industrial and Applied Mathematics (SIAM): Philadelphia, PA, USA, 2005. [Google Scholar]